Lake Store Finnsjøen - a key for understanding Late-Glacial/early Holocene vegetation and ice sheet dynamics in the central Scandes Mountains

Aage Paus[a], Sanne Boessenkool[b1], Christian Brochmann[b], Laura Saskia Epp[b2], Derek Fabel[c], Haflidi Haflidason[d], Henriette Linge[d].

[a] Department of Biology, University of Bergen, P.O. Box 7803, Thormøhlens gate 53 A, NO-5020 Bergen, Norway

[b] Natural History Museum, University of Oslo, P.O. Box 1172 Blindern, NO-0318 Oslo, Norway

[c] School of Geographical and Earth Sciences, University of Glasgow, Glasgow G12 8QQ, Scotland, U.K.

[d] Department of Earth Science, University of Bergen, and Bjerknes Centre for Climate Research, Postbox 7803, NO-5020 Bergen, Norway

[1] Present address: Centre for Ecological and Evolutionary Synthesis, Department of Biosciences, University of Oslo, P.O. Box 1066, Blindern, NO-0318, Oslo, Norway

[2] Present address: Alfred Wegener Institute Helmholtz Centre for Polar and Marine Research, Periglacial Research, Am Telegrafenberg A43, 14473 Potsdam, Germany

Corresponding author:

Aage Paus, Department of Biology, University of Bergen, P.O. Box 7803, Thormøhlens gate 53 A, NO-5020 Bergen, Norway. Phone: + 47 55 58 33 44. Fax: + 47 55 58 96 67. E-mail: aage.paus@uib.no

Key words**:**
stratigraphy; pollen; sedimentary ancient DNA; vegetation development; AMS dates; Beryllium-10 surface exposure ages; Late-Glacial; early Holocene; deglaciation; ice models; Alpine Central Norway; Scandes

Abstract

The Late-Glacial (LG) deglaciation and vegetation development in the Scandes Mountains has been debated for a century. Here we present new evidence from microfossils, radiocarbon dated plant macrofossils and sedimentary ancient DNA from laminated sediments in Lake Store Finnsjøen (1260 m a.s.l.) at Dovre, Central Norway. Combined with previous results from three other Dovre lakes, this allows for new interpretations of events during and immediately after the LG deglaciation. The Finnsjøen sediments present the first uninterrupted record of local vegetation development in the Scandes Mountains from the late Younger Dryas (YD), ca 12,000 cal years BP, to the early Holocene around 9700 cal years BP. The local vegetation in late YD/early Holocene was extremely sparse with pioneer herbs (e.g. *Artemisia norvegica, Beckwithia, Campanula cf. uniflora, Koenigia, Oxyria, Papaver, Saxifraga* spp.) and dwarf-shrubs (*Betula nana, Salix* including *S. polaris*). From 11,300 cal years BP, local vegetation rapidly closed with dominant *Dryas, Saxifraga* spp., and *Silene acaulis*. From ca 10,700 cal years BP, open birch-forests with juniper, *Empetrum nigrum* and

other dwarf-shrubs developed. Pine forests established within the area from 10,300 cal years BP. We identified the cold Preboreal Oscillation (PBO), not earlier described from pollen data in South Norway, around 11,400 cal years BP by a regional pollen signal. Distinct local vegetation changes were not detected until the post-PBO warming around 11,300 cal years BP. Apparently, the earlier warming at the YD/Holocene transition at 11,650 cal years BP was too weak and short-lived for vegetation closure at high altitudes at Dovre. For the first time, we demonstrate a regional glacier readvance and local ice cap formations during the YD in the Scandes Mountains. In two of the deep lakes with small catchments, YD glaciation blocked sedimentation without removing old sediments and caused a hiatus separating sediments of the ice-free LG interstadial (LGI) from those of the ice-free Holocene period. Both regional glaciers and local ice caps caused hiati. Ice-free pre-YD conditions at Dovre followed by a YD readvance point to a scenario that is intermediate between the maximum ice model postulating a thick glacier during the entire LG, and the minimum ice model postulating thin and multi-domed early LG ice.

1. Introduction

The thickness of the Scandinavian ice-sheet during the Weichselian, the time of the deglaciation, and the development of ecosystems during and immediately after deglaciation have long been debated. Today, the maximum ice model postulating one massive central ice-dome present until the early Holocene (e.g. Holtedahl, 1955; Vorren, 1977; Andersen, 1981; Mangerud, 2004), has been challenged by the minimum ice model involving a fluctuating and thin multidomed ice-sheet (e.g. Lambeck et al., 1998, 2010; Arnold et al., 2002; Wohlfarth, 2010). In accordance with the minimum model, the alpine region of Central Norway has been

assumed by several authors as deglaciated during the Late-Glacial (LG) before the Younger Dryas (YD) cold period (Dahl et al., 1997; Paus et al., 2006, 2011, 2014; Bøe et al., 2007; Goehring et al., 2008). In contrast, other authors rather interpreted glacial lineations and moraines at high altitudes in this region to reflect northeastern and northwestern ice flows in the YD supporting the maximum ice model (Follestad, 2005; Follestad and Fredin, 2007; Olsen et al., 2013, 2014).

As no consensus has been reached regarding the time of Scandes Mountains deglaciation (Fig. 1) due to the lack of reliable radiocarbon dates, the immigration of species and their establishment during the LG have been debated (e.g. Kullman, 2002 *vs* Birks et al., 2005). Also, due to fragmentary and incomplete early Holocene sediment sequences, the Scandes vegetation development from pioneer vegetation to forests in the following periods is not known in detail (Giesecke, 2005; Paus, 2010; Paus et al., 2011). For example, we know little about how vegetation responded to the early Holocene climate oscillations (Hoek and Bos, 2007; Paus, 2013) or when the earliest forests established in the Scandes Mountains.

In order to test the models on ice thickness, time of deglaciation, and immigration of plants to newly deglaciated areas at Dovre, we studied sediments from a new lake: Lake Store Finnsjøen, 1260 m a.s.l. (Fig. 1). This lake is situated close to and between Lake Ristjønna (1253 m.a.s.l.) and Lake Topptjønna (1316 m a.s.l.) studied by Paus et al. (2011) and 30 km west of Lake Flåfattjønna (1110 m a.s.l.) studied by Paus et al. (2006) and Paus (2010) (Fig. 1). We utilized microfossil analysis, ^{14}C-dating (AMS) of plant macrofossils, lithostratigraphy (LOI, X-ray, tephra) and sedimentary ancient DNA (sedaDNA) from deglacial sediments, as well as surface exposure dating with the terrestrial cosmogenic nuclide (TCN) ^{10}Be. In addition, we merged the pollen data from the four studied Dovre lakes and treated them by

PCA ordination. Our new data together with the previously published data on the other lakes at Dovre enabled new interpretations of events during and immediately after the LG deglaciation of Dovre.

2. Regional setting

The Dovre mountain ridge with Lake Store Finnsjøen and the previously studied lakes (Topptjønna and Ristjønna; Paus et al., 2011) is situated between the valleys Drivdalen and Vinstradalen in Sør-Trøndelag County, Central Norway (Fig. 1). Lake Flåfattjønna lies 30 km to the east of the ridge (Paus et al. 2006; Paus 2010). Features of the four lakes in the Dovre study are listed in Table 1.

The Finnsjøen sediments were cored close to Mt. Finnshø in a 14-15 m deep lake bottom depression with a diameter of 60-70m. Beyond the depression, the lake is not deeper than 6 m. The bedrock comprises a number of geological units belonging to the Røros nappe complex (Krill, 1987; Nielsen and Wolff, 1989). The northern part of the mountain ridge, where Ristjønna is located, consists of augen gneiss, quartz-feldspar slate, and calcareous mica schist. The southern part of the ridge, where Finnsjøen and Topptjønna are located, consists of greenschist/-stone, slate and hornblende amphibolite. On the mountain ridge, there is a mixture of continuous and discontinuous till covers, and rogen moraines are situated east of and adjacent to Finnsjøen (Sollid et al., 1980).

The mountain ridge is situated in the upper low-alpine zone with lichen-dominated dwarf-shrub tundra with *Empetrum nigrum s.l.*, *Vaccinium* spp., and *Betula nana.* The calciphilous

Artemisia norvegica, Campanula uniflora, Dryas octopetala, and *Salix polaris* also occur there, and *Juniperus communis* and *Salix* shrubs are found at protected sites.

The regional climate is continental with July and January mean temperatures of ca. 7.5-8 °C and -11 °C, respectively and an annual precipitation of 450 mm. The temperatures have been estimated using data from the nearest climate stations at Kongsvold and Fokstugu (DNMI, 2015), assuming a lapse rate of 0.6 °C /100 m (Laaksonen, 1976). The regional forest-line of *Betula pubescens* is situated at about 1050-1100 m a.s.l. In continental areas such as Dovre, the forest-line roughly follows the 10 °C July isotherm (Odland, 1996).

3. Material and methods

3.1. Sampling and lithostratigraphy

The Finnsjøen lake sediments were retrieved at maximum water depth (14.7 m; UTM coordinates: NQ 32V 0535133 6918753) by coring from winter-ice. We used a 110 mm piston corer (Nesje, 1992) modified by A. Paus and J. Kusior (Dept. of Earth Science, Univ. of Bergen), which allowed us to use 6 m tubes and start coring several meters below the sediment surface. The results presented in this paper are based on the lowermost core section (1980-2195 cm depth below water surface) with 4 cm basal faint laminated clay gyttja (2191-2195 cm depth) below a minerogenic part of 103 cm and an upper 108 cm organic part distinctly laminated by macrofossil layers (Fig. 2). These sediments were described (Table 2) according to the method of Troels-Smith (1955). We were unable to core deeper, as the corer became totally filled with sediments.

149 The percentage loss-on-ignition (LOI) was measured in 2-10 cm from the studied core section
150 1980-2195 cm. The subsamples were dried overnight at 105 °C, weighed and ignited at 550
151 °C for 1 h. The weight LOI was calculated as % of dry weight.
152
153 To document the sediment structure in the minerogenic part of the core, sediments were X-ray
154 photographed using Philips X-ray 130 kV instrument. The X-ray imagery was processed on a
155 negative film. The results were later transferred into a positive format using a digital camera
156 (Fig. 2).
157
158 Tephra particles were searched for in every 5 cm in the minerogenic bottom part of the core.
159 Particularly, we looked for tephra particles from the regional Vedde Ash layer (12.1 cal ka
160 BP; Grönvold et al., 1995; Bondevik et al., 2001). Samples were collected, sieved on different
161 sieves down to 30 micron, and studied under a microscope. However, no tephra particles were
162 found.
163
164
165 *3.2. Pollen*
166 Material for pollen analysis was sampled at 1–4 cm intervals below 2080 cm and 20 cm above
167 (Fig. 3). The samples were treated with HF and acetolysed according to Fægri and Iversen
168 (1989). In addition, after each treatment with HCl or KOH, the pollen samples were
169 centrifuged for 7-8 cycles in water to achieve clean samples from the lime-rich minerogenic
170 sediments. *Lycopodium* tablets were added to the samples (1 cm^3) for estimates of
171 concentration and influx (Stockmarr, 1971). Identifications were based on Fægri and Iversen
172 (1989), Moore et al. (1991), and Punt et al. (1976-1996), in combination with a reference
173 collection of modern material. *Betula nana* pollen was distinguished using the morphological

criteria of Terasmäe (1951). In the pollen diagram (Fig. 3), the percentage calculation basis (ΣP) comprises the terrestrial pollen taxa. For a taxon X of aquatic plants (AQP) and spores, the calculation basis is ΣP+X. The pollen diagram was divided into local pollen assemblage zones (paz) by visual inspection. The computer program CANOCO 4.5 (ter Braak and Smilauer, 1997-2002) was used for detecting and graphing ordination patterns in the terrestrial vegetation development (Fig. 4) based on a data set including pollen results from lake Store Finnsjøen merged with results older than ca 9.5 cal ka BP from Lake Flåfattjønna (1447 – 1552 cm depth), Lake Ristjønna (1233 – 1320 cm depth), and Lake Toppjønna (784 – 937 cm depth) (Paus et al., 2006, 2011).

Palynological terrestrial richness (PR) was estimated by rarefaction analyses (program RAREPOLL, Birks and Line, 1992) using Σ terrestrial microfossils = 124 as the statistical base ($E(T_{124})$). Due to the low statistical basis, the PR estimates do not strongly indicate the total floristic richness within the pollen source area. Intermediate levels of disturbance maximize richness by preventing both dominance and extinction of species (Grime, 1973). In accordance with this, the low estimated terrestrial PR $E(T_{124})$ when the abundance of tree pollen (AP) is high (Fig. 3), should indicate closed forests, whereas local PR maxima indicate periods when the vegetation was positioned close to and above forest-lines (e.g. Aario, 1940; Simonsen, 1980; Seppä, 1998; Grytnes, 2003).

3.3. sedaDNA analyses

A total of 43 samples were successfully analysed for *sed*aDNA, and 17 of these were from the lowermost core section that is the focus of the present study. All analyses presented below are based on all 43 samples that yielded DNA, but the presented results are limited to the 17 samples relevant to this study (see Appendix A for sample details). The DNA samples were

199 taken from the inside of the core, after removing one half of its casing (see supplementary
200 methods in Appendix A for details).
201
202 DNA was extracted as described in Boessenkool et al. (2014). PCRs (25 µL) contained 2 µL
203 DNA, 0.2 µM of each primer, 1 mM dNTPs, 0.8 mg / mL bovine serum albumin (BSA), 2
204 mM $MgSO_4$, 1x PCR buffer and 1.25 U Platinum®Taq DNA polymerase High Fidelity
205 (Invitrogen). The amplification profile consisted of 2 min at 95 °C, 45 cycles of 30 s at 95 °C,
206 30 s at 50 °C and 30 s at 68 °C, followed by a final extension of 10 min at 72 °C. Samples
207 were amplified using the *trn*L *g* and *h* primers (Taberlet et al., 2007). Primers were modified
208 on the 5' end with unique 8 bp tags that differed from each other in at least 5 basepairs, and
209 were preceded by NNN to improve cluster generation on the sequencer (Coissac, 2012; De
210 Barba et al., 2014). PCR products were visualized on agarose gels. For each sample, up to five
211 PCRs were performed and whenever possible three positive amplifications were pooled for
212 sequencing. Pooled PCR products were purified with MinElute (Qiagen) and quantified using
213 a Qubit® 2.0 fluorometer (Invitrogen). An equimolar mixture of all PCR products was
214 sequenced on an Illumina Miseq (paired-end 2x100 bp) at Fasteris (Switzerland).
215
216 Extractions and PCR setup were performed in a dedicated aDNA laboratory at the Natural
217 History Museum (University of Oslo). Established ancient DNA precautions to minimize
218 contamination were adhered to throughout the experiments (Willerslev et al., 2004; Willerslev
219 & Cooper, 2005). See supplementary methods in Appendix A for details, including a list of
220 the sequences that were removed from the dataset, because they were identified to cultivated
221 taxa and/or were extremely unlikely to occur in the study area.
222
223 Sequence data were analysed using a suite of programs from the OBITools package

(http://metabarcoding.org/obitools). The programs *solexapairend* and *ngsfilter* were used to assemble forward and reverse reads, and to remove reads with any errors in the tags or with more than two errors in the primer sequences. Subsequently, all reads < 10 bp in length were removed with the program *obigrep*, and identical reads were merged (100% coverage required) using *obiuniq*. Finally, *obiclean* was used to remove putative PCR and sequencing errors. For taxonomic assignment, we used the program *ecoTag* and analyzed the sequences against two taxonomic reference libraries: 1) a combined curated library containing the Arctic and Boreal vascular plant libraries and the Arctic-boreal bryophyte library (containing 1664 vascular plant species and 486 bryophyte species; Sønstebø et al., 2010, Willerslev et al., 2014; Soininen et al., 2014) and 2) a reference library based on the embl standard sequences release 113 (see Boessenkool et al. 2014). Initially, only sequences represented by more than 100 reads and with an identity > 0.95 were kept in the final dataset, but after the observation of chimeric sequences (see above) we removed any sequences within a sample that were represented by < 400 reads in that specific sample. All analyses were done using computing facilities provided by the Norwegian Metacenter for Computational Science (Notur). Final assigned taxonomic identities can be found in Appendix A, and the output from the program ecoTag (including the sequences) can be found in the Appendices B and C.

3.4. Radiocarbon dating and age-depth modelling

Seven samples of terrestrial plant remains from the Store Finnsjøen organic sediments above 2188 cm depth were AMS radiocarbon-dated (Table 3). As no datable macrofossils were found in the minerogenic sediments below, the LG chronology in these sediments is based on assumed ages. All dates are given in calibrated years BP (cal BP; present = 1950 AD) based

248 on the InCal13 calibration curve (Reimer et al. 2013). The dates were converted to calendar
249 ages using CALIB 7.02 (Stuiver et al., 2014).
250
251 To model the best fit age-depth relationships (Fig. 5) based on the available ^{14}C ages we used
252 the "Bacon" approach (Blauuw and Christen, 2011). Except for dividing the short Finnsjøen
253 core into 2 cm sections (default is 5 cm), we used default settings.
254
255 *3.5. ^{10}Be surface exposure dating*
256 Four samples were collected from bedrock surfaces in the Lake Flåfattjønna area (Fig. 1) for
257 surface exposure dating with *in situ* cosmogenic ^{10}Be. All samples were taken from bare
258 surfaces with exposed quartz veins or lenses in phyllite/ mica schist. The two lower elevation
259 surfaces showed evidence of ice moulding and glacial deposition (boulders), whereas the two
260 higher elevation surfaces appeared glacially plucked (Fig. 6). Field observations are listed in
261 Table 4A. The rock samples were processed for surface exposure dating (following
262 procedures modified from Child et al. (2000)) at the School of Geographical and Earth
263 Sciences (University of Glasgow), and at the Cosmogenic Isotope Laboratory at the Scottish
264 Universities Environmental Research Centre (SUERC). Resulting Be targets were measured
265 at the SUERC AMS laboratory (Xu et al., 2010).
266
267 Surface exposure ages were calculated from ^{10}Be concentrations using the CRONUS-Earth
268 online calculator (Balco et al., 2008; CRONUS-Earth, 2015). Table 4A and B show the
269 relevant field and laboratory data, as well as the calculated surface exposure ages. The surface
270 exposure ages were calculated according to the Lm scaling scheme using 1) the global
271 average ^{10}Be production rate (spallation-induced production of 4.39±0.37 atoms g^{-1} a^{-1}, Balco
272 et al., 2008), 2) the western Norway ^{10}Be production rate from Goehring et al. (2012)

(spallation-induced production of 4.07±0.16 atoms g^{-1} a^{-1}, Alternate calibration data sets, CRONUS-Earth (2015)), and 3) the Arctic ^{10}Be production rate from Young et al. (2013) (spallation-induced production of 3.93±0.15 atoms g^{-1} a^{-1}, Alternate calibration data sets, CRONUS-Earth (2015)).

4. Results

4.1. Lithostratigraphy (Table 2, Fig. 2)

The core section presented in this study (1980-2195 cm) is distinctly laminated (Fig. 2). In the organic part above 2088 cm, the laminations are primarily dark layers of macrofossils, though a few lighter silt/clay horizons occur. Below the homogenous silty clay sediments at 2088-2115 cm depth and older than ca 11.65 cal ka BP (extrapolated; see Fig. 5), a 70 cm thick clay-rich layer (2115-2185 cm depth) shows ca 250 laminations according to a high resolution X-ray photo imagery (Fig. 7). In the upper part, the lamina thickness is ca 3 mm, in the lower part it is ca 5 mm. The bending of laminas was apparently formed during coring and reflects the sediment softness and viscosity when saturated by water. A dark and stratified sorted sand layer occurs at 2185-2191 cm depth, between the laminated clay above and a laminated silty clay gyttja below (Fig. 8).

4.2. Pollen results and statistical analysis (Figs. 3 and 4, Table 5)

A total of 94 terrestrial taxa were identified in 45 levels of the Finnsjøen sediments. The pollen concentrations in paz 2, 3 and 4 were extremely low (in some levels down to 50 grains cm^{-3}). Even when samples were analysed for two or three days, the mean sum of terrestrial pollen (ΣP) per sample did not reach more than 339 grains. The absence of corroded pollen

298 grains throughout the sedimentary sequence indicates negligible content of reworked material.
299 Six local pollen assemble zones were defined (Fig. 3, Table 5).
300
301 A data set that included the merged pollen results from Lakes Finnsjøen, Ristjønna,
302 Topptjønna, and Flåfattjønna was subjected to a DCA ordination that showed a gradient
303 length of 1.87 standard deviation units of turnover. This suggested linear response curves.
304 Hence, PCA was chosen as ordination technique. In the graph of the two first PCA axes, the
305 light-demanding pioneers are concentrated to the right (Fig. 4). Among these, taxa on well-
306 drained disturbed soils (e.g. *Artemisia* spp., Poaceae) were more frequent in the lower part of
307 the graph, whereas snow-bed plants (e.g. *Oxyria*-type, *Saxifraga oppositifolia*-type) were
308 found in the upper right. Trees and shrubs such as juniper and tree-birch dominated to the left.
309
310 *4.3. Taxa identified by sedaDNA (Table 6).*
311 The sequencing run provided 13 351 142 sequence reads that could be correctly assembled
312 with no errors in the tags and not more than 2 errors in the primer site sequences. After further
313 filtering on sequence length and removal of putative PCR and sequencing errors, 10 307 634
314 reads representing 2 278 unique sequences remained. A total of 89 unique sequences (8 199
315 825 reads) could be identified using our combined Arctic-boreal reference library with
316 similarity >0.95 and a total representation of >100 reads. Using the embl databases, we
317 identified 122 unique sequences (9 963 948 reads). Sequences with similarity <1.00 (but
318 above 0.95) were checked manually against the closest matching reference sequences. For
319 genera for which not all the relevant species were included in our library, we adjusted any
320 identification to the species level up to the genus level. Similarly, we were able to narrow
321 down some identifications by excluding Beringian/American species.
322

Ten out of the 16 samples from the lowermost core section showed positive amplification and were included in the sequencing run. Eight of these samples contained sequences that passed all filtering steps, resulting in identification of a total of 14 taxa (Table 6). Taxonomic resolution varied from family to species level. The *trn*L *g* and *trn*L *h* primers are designed for vascular plants but also amplify bryophytes, and we recovered DNA from one bryophyte genus (*Splachnum* sp.) in our samples. The number of taxa identified from each sample varied from one to seven, with the oldest samples containing the least diversity.

The DNA data confirmed and complemented the records of pollen and spores. The *Rhinanthus* pollen type seemed to be represented by *Bartsia alpina* in the DNA data, whereas the retrieval of *Arbutoideae* DNA probably corresponded to pollen finds of *Arctous* and *Arctostaphylos*. For several taxa, the DNA data increased the taxonomic resolution relative to pollen data (e.g. *Bistorta vivipara, Pinus sylvestris*).

4.4. ^{10}Be surface exposure ages (Table 4)

In this study, we use the results obtained using the Arctic production rate because its calibration data set extends back to ca. 16 ka. When comparing surface exposure age results internally, the analytical uncertainties (parentheses in age results column, Table 4B) should be used, whereas we use the full uncertainty when comparing ^{10}Be ages with dating results obtained using other methods.

The resulting ^{10}Be surface exposure ages appear to increase with increasing elevation (cf. Linge et al., 2006). The two lower-elevation surfaces yield overlapping ^{10}Be ages and are thus not statistically different. The same is the case for the two higher-elevation surfaces. There is, however, a clear difference in results for the two elevation levels with 10.9 and 11.3 ka (mean

11.1±0.5 ka) *versus* 21.6 and 21.9 ka (mean 21.7±0.8 ka). Single nuclide surface exposure dating provides the apparent exposure age of rock surfaces, but does not confirm whether the surface exposure has been continuous or occurred during multiple episodes. Moreover, ages based on single nuclide measurements do not reveal possible subglacial erosion that could have removed previously accumulated nuclides. The geomorphic settings suggest that the lower sampling locations were glacially scoured, whereas the summit was plucked. The two lower-elevation samples are considered to reflect the timing of final deglaciation, whereas the summit samples suggest insufficient subglacial erosion to remove nuclides from prior exposure.

5. Discussion

The Finnsjøen multi-proxy data (spanning from ca 9.7 to > 12.85 cal ka BP) presented in this study provides evidence of a previously undescribed LG deglaciation landscape and vegetation establishment in the Scandes Mountains. We emphasize however, that the LG chronology is exclusively based on stratigraphical correlations and considerations. We discuss the Lake Store Finnsjøen sediments and chronology (section 5.1.), the Lake Store Finnsjøen palaeoenvironment (section 5.2.), the stratigraphies of the four Dovre lakes (section 5.3.), and the Dovre deglaciation dynamics (section 5.4) with the interpretations in each section based on the conclusions of the previous section. Finally, we combine all evidence in the concluding section.

5.1. Lake Store Finnsjøen – sediments and chronology (Figs. 2, 7, 8, and 9)

373 The ^{14}C ages show a linear age/depth relationship, reflecting a rapid sediment accumulation
374 (12 yrs/cm) for the organic deposits between ca 11.3 and 10 cal ka BP (Fig. 5). Apparently,
375 the restricted depression where the coring was carried out was effectively filled up by
376 inwashed organic material. Hence, sediment focusing is most probably involved. Though,
377 minerogenic sediments may not be strongly focused according to Davis et al. (1984).
378
379 The laminated clay unit located below the organic sediments (Fig. 7) is similar to sediments
380 found in present polar desert lakes in Arctic Canada (K. Gajewski and S. Lamoureux, pers.
381 comm.). These lakes have a more-or-less permanent ice cover and a moat (littoral band of
382 open water) that varies in size from year to year. A semi-permanent ice cover at Finnsjøen is
383 consistent with the low frequencies of algae, pollen, and sedaDNA (Fig. 3, Table 5), as ice
384 cover strongly reduces light transparency and limits the open-water depositional surface. Such
385 low frequencies also suggest that the laminations cannot be biogenetic (cf. Perren et al., 2003;
386 Paasche and Larsen, 2010) and must have a clastic origin. The weakly developed and fine-
387 grained laminations show a stable and low-energy depositional environment, too weak to
388 indicate impact from regional glaciers (cf. Zolitscka, 2007; Larsen et al., 2012; Ojala et al.,
389 2012). Instead, the laminations could point to rhythmic variations in (1) moat-size and/or (2)
390 run-off from local glaciers/snow-beds within the restricted catchment of Finnsjøen (cf. Brauer
391 and Casanova, 2001; Zolitscka, 2007) which suggests the laminations may represent seasonal
392 variations (varves). The ca. 250 laminations found below the biostratigraphic signal of the
393 onset of the Holocene at 11.65 cal ka BP (Figs. 5, 7) would then show that the Finnsjøen
394 varve deposition started during the late YD, not later than 11.9 cal ka BP. The decreasing
395 lamination thickness from 5 mm in the lower part to 3 mm towards the top (2115 cm) most
396 probably indicate an increasing distance from the active local ice still present within the lake
397 catchment (Zolitschka, 2007). Laminations are absent in the homogenous silty clay above

(2115-2088 cm) which might indicate the total melt of the local ice cap around the onset of the Holocene according to the age-depth model (Fig. 5).

The sand layer (2185-2191 cm depth) just below the laminated clay (Fig. 8) was probably rapidly deposited around 12 cal ka BP. In line with this, the absence of Vedde Ash indicates that the layer is younger than 12.1 cal ka BP (Bondevik et al., 2001). At 2191 cm depth, simultaneous and extremely abrupt changes occur in (1) the lithostratigraphy, from the sand layer to a 5 mm light clay horizon below (Fig. 8), (2) the pollen assemblages, i.e. the paz F-1/F-2 transition (Fig. 3), (3) the pollen concentrations, which are about 10-100 times higher in paz F-1 than in paz F-2, and (4) the loss-on ignition (Fig. 3). We think that these coinciding stratigraphical events must reflect a hiatus. The hiatus separates an upper YD biostratigraphy from a distinctly different pollen assemblage below, pre-dating YD and quite similar to the LGI assemblages of the adjacent Dovre lakes Topptjønna and Ristjønna where local ice caps did not develop (Paus et al., 2011). Evidence from the Greenland ice cores shows that the YD started 12.85 cal ka BP (Rasmussen et al., 2006; Thomas et al., 2007), so the hiatus must span at least 900 years. We think that the hiatus represents the YD establishment of a local ice cap blocking sedimentation and that the sand layer reflects the start of the ice melting in the late YD (see below). The local ice cap did not erode the underlying sediments, as laminations below the hiatus/sand layer including the uppermost light clay horizon are complete and intact (Fig. 8). The lake and catchment topography appear to have prevented water and water saturated sediments to escape, when the local ice cap blocked the lake.

5.2. Finnjøen Late Glacial and early Holocene palaeoenvironment

5.2.1. The Late Glacial Interstadial, paz F-1 (> 12.85 cal ka BP)

Paz F-1 (Fig. 3, Table 5) correlates to the tree-pollen dominated period at Dovre (Fig. 9) interpreted to reflect the Late Glacial Interstadial (LGI) (Paus et al., 2011). The local vegetation included mosaics of shrub/dwarf-shrub tundra (with e.g. *Alnus, Hippophaë, Juniperus, Salix* sp., *Betula nana, Empetrum*), grasslands (Poaceae, *Parnassia, Ranunculus acris, Rumex*), snow-beds (*Oxyria, Saxifraga*), and windblown ridges (*Arctous, Artemisia, Dryas*) expressing variations in topography, snow cover, and shelter. This vegetation was similar to and as diverse as the present low-/mid-alpine vegetation of Dovre. Mean July temperatures of at least 7-8 °C, similar to today, are suggested by the local presence of juniper, dwarf-birch, and *Parnassia* (Kolstrup, 1979; Paus et al., 2003). In addition, well-represented *Pediastrum* and *Botryococcus* suggest the lake was ice-free during summers.

5.2.2. Late Younger Dryas, paz F-2 (ca. 12 – ca. 11.65 cal ka BP)

Across the hiatus that corresponds to the paz F1/F2 transition (section 5.1.), total pollen concentrations drop to max. 800 grains cm^{-3}, less than one tenth of the concentrations in paz F-1. Assuming that paz F-2 lasted ca 350 years (ca. 12 - ca.11.65 cal ka BP), a tentative total pollen accumulation rate (TTPAR) can be estimated to 50-80 grains cm^{-2} a^{-1}, which is similar to that of contemporary mid-arctic tundra (Ritchie and Lichti-Federovich, 1967; Fredskild, 1973). PR shows high species richness in open vegetation (Fig. 3). The occurrence of *Papaver radicatum*, *Artemisia* cf. *norvegica*, *Campanula* cf. *uniflora*, and *Dryas* reflects windblown ridges, whereas *Beckwithia glacialis, Oxyria, Saxifraga* and dwarf *Salix* (one *S. polaris* leaf found) show extensive snow-beds. *Thalictrum* and *Selaginella* suggest moist grasslands. Similar open YD pioneer vegetation has been described from Lakes Topptjønna and Ristjønna at Dovre (Paus et al., 2011). The low TTPAR and the dominance of pioneer plants (Fig. 3) strongly suggest that pine and tree-birch are mostly long-distance represented. However, pine

447 stomata (Paus et al., 2011) and the constant F-2 representation of well-preserved *Picea abies*
448 grains (Fig. 3) could indicate their YD presence within the Dovre region (Paus et al., 2011).
449
450 SedaDNA is primarily local in origin (Jørgensen et al. 2012), and is therefore considered to
451 mainly reflect local vegetation. The low number of taxa retrieved from the sedaDNA analysis
452 (Table 6) therefore suggests a sparsely developed local flora. The high PR could then reflect
453 extra-local or regional pollen. However, the limited sedaDNA retrieved from this layer may
454 also be a consequence of post-mortem degradation of DNA, which leads to a decline in
455 diversity with sample age (e.g. Boessenkool et al., 2014).
456
457 The low algae representation (Fig. 3) suggests cold water and/or reduced access to light in a
458 lake with ice-free moats during summers (see section 5.1.). Between 2166 and 2150 cm water
459 depth, the algal representation increased, and diatoms were observed during the search for
460 tephra. This might reflect a milder period and broader moats, improving light transparency in
461 the water. In Arctic Canada today, incomplete melting of lake-ice occurs in areas with July
462 means of 3-5 °C and annual means of -17° to -19 °C (Belzile et al., 2001; Cook and Bradley,
463 2010), similar to the YD conditions on Greenland (Denton et al., 2005).
464
465 5.2.3. The onset of the Holocene, paz F-3 (ca. 11.65 - ca.11.45 cal ka BP)
466 The rapid tree-birch increase at the expense of open ground pioneers likely reflects regional
467 changes in response to the ameliorating Holocene climate ca. 11.65 cal ka BP (Rasmussen et
468 al., 2006; Thomas et al., 2007) as similarly signalled south and west of the Scandinavian ice
469 sheet (e.g. Hafsten, 1963; Paus, 1995; Krüger et al., 2011). TTPAR (80-100 grains cm^{-2} a^{-1})
470 similar to that of paz F-2, still indicates the local presence of a mid-arctic tundra (Ritchie and
471 Lichti-Federovich, 1967; Fredskild, 1973). Accordingly, the distinct *Betula* and *Populus*

representation in paz F-3 most probably reflects long-distance transport from favourable down-slope areas within the region. *Pediastrum* and *Botryococcus* show maxima at the paz F-3/F-2 transition, reflecting temporary ameliorating conditions for algal growth.

5.2.4. The Preboreal oscillation (PBO), paz F-4 (ca. 11.45-11.3 cal ka BP)

The increase in open ground pioneers at the expense of tree-birch in the paz F-4 reflects a vegetation setback (Fig. 3, Table 5). As TTPAR (40-70 grains cm^{-2} a^{-1}) is not statistically different from that of paz F-3, we think that the distinct pollen percentage changes (e.g. the *Betula* decrease) mostly reflect a regional vegetation setback whereas the local mid-arctic tundra stayed more or less similar to those of paz F-3 and paz F-2. The paz F-4 changes including the regional tree-birch decrease are interpreted to reflect the PBO cooling (Björck et al., 1997) dated to ca. 11.4 cal ka BP (Hoek and Bos, 2007; Rasmussen et al., 2007). Currently, the PBO has only been recognized at a few sites in southern Norway (Bakke et al., 2005, Nesje et al., 2014).

5.2.5. The pre-pine local successions, paz F-5 (ca. 11.3 – ca. 10.3 cal ka BP)

The pollen assemblage reflects closing of local vegetation as also indicated by declining PR (Fig. 3). The sedaDNA data show increasing number of taxa (Table 6), which could indicate efficient outwash from the increasing vegetation cover within the catchment. However, we cannot exclude that the sedaDNA increase reflects less degradation in the younger and more organic F-5 deposits. In paz F-5A (11.3-10.7 cal ka BP), *Dryas* and *Silene acaulis* expanded on the ridges at the expense of *Artemisia*, whereas widespread snow-beds with dominant *Salix* (including *S.polaris*; Table 3), *Saxifraga*, and possibly *Equisetum* developed (Fig. 3, Table 6). SedaDNA occasionally seems to originate from wind-dispersed pollen (Boessenkool et al. 2014), and the DNA of Fagaceae (Table 6) most probably reflects long-distance *Quercus*

pollen (Fig.3). A sudden increase in total accumulation rate (TPAR) from 70 to 400 grains cm^{-2} a^{-1} at the F-4/F-5A transition and further to 2000 grains cm^{-2} a^{-1} at the end paz F-5A reflects a development from mid-Arctic via low-Arctic tundra to forest-tundra (Ritchie and Lichti-Federovich, 1967). However, frequent macrofossil layers show efficient deposition and focusing that leads to over-estimated PAR values (Davis et al., 1984).

In F-5B (ca. 10.7 – ca. 10.3 cal ka BP), TPAR increased to 3000 grains cm^{-2} a^{-1} showing further vegetation closure. Decreasing *Saxifraga* and maxima in *Juniperus* and dwarf-shrubs suggest drier soils. The 1% ΣP *Hippophaë* could reflect local stands indicating a July mean of 11-12 °C (Kolstrup, 1979). The identification of pine from sedaDNA (Table 6) supports previous pine stomata and megafossil finds from Dovre (Paus et al., 2011), but we cannot exclude long-distance representation from pollen. The tree-birch pollen reached 1200 grains cm^{-2} a^{-1}, which is sufficient to indicate local forests (Seppä and Hicks, 2006; Jensen et al., 2007). However, focusing may have reduced the evidential strength of PAR (see above). Overall, the F-5 successions show identical patterns to what is found in the early Holocene in other Dovre sites (Velle et al., 2005; Paus et al., 2006, 2011; Paus, 2010).

The initiation of the local terrestrial paz F-5 successions is simultaneous with abrupt rises in *Pediastrum*, *Botryococcus* and LOI (Fig. 3) and the sudden change from blue-grey silty clay to brown clay/silt gyttja (Table 2). We hypothesise that these coinciding events reflect a rapid warming at 11.3 cal ka BP and the total melt of lake-ice during summers, which improved light conditions and algal growth. This is the first typical "YD/Holocene" stratigraphical signal evident in the analysed core, suggesting that the warming at the YD/Holocene transition at 11.65 cal ka BP was too weak and short-lived to leave distinct traces at the high

altitudes at Dovre. Similar patterns have been indicated from other Dovre lakes (Paus, 2010; Paus et al., 2011).

5.2.6. Pine-forest establishment, paz F-6 (ca. 10.3 – ca. 9.7 cal ka BP)

The rapid PR-drop and strong pine rise (8 x 10^3 grains cm^{-2} a^{-1}) show that pine forests established locally and simultaneously with the regional pine-forest expansion (Owren, 1984; Høeg, 1994), as also shown by previous megafossil finds (Paus, 2010; Paus et al., 2011). Ten cal ka old tree-birch seeds (Table 3) indicate local trees, whereas open patches are shown by well-represented dwarf-shrubs and herbs (Fig. 3, Table 6). Pine DNA was not detected in F-6, but the effect of different sources of bias on the taxa recovered by sedaDNA is still largely unclear (see e.g. Boessenkool et al. 2014), and lack of detection is therefore difficult to interpret.

5.3. Correlation of the Dovre lake stratigraphies (Figs. 9 and 10)

When comparing the LG/early Holocene biostratigraphies (PCA, total pollen diagram) of the four Dovre lakes Flåfattjønna (Paus et al., 2006; Paus, 2010), Topptjønna and Ristjønna (Paus et al., 2011), and Finnsjøen (this study), three main periods can be recognized:

(1) The undated pre-YD characterized by low PCA1 and PCA2 values, high tree-pollen percentages and (except for Flåfattjønna) closed vegetation on well-drained soils. The continuous and uninterrupted minerogenic sedimentation in Ristjønna (see below) suggests that period 1 represents the LGI. This is further supported by the poor organic content of the sediments (making it unlikely that the sediments represent the warm Eemian period), and by the pollen assemblage that differs strongly from adjacent interstadial signals older than the LG (Helle et al., 1981; Lie et al., 2004; Paus et al., 2011).

(2) The YD to the end of the PBO, showing medium PCA2 values, maximum PCA1 values, medium to low tree-pollen percentages, dominant *Artemisia* and Poaceae, and pioneer vegetation on well-drained soils. Within this period, the YD/Holocene transitions are found in minerogenic sediments (Fig. 9). Most interestingly, the sediments in the easternmost lake, Flåfattjønna, lack this YD-PBO period (see below).

(3) The early Holocene after the PBO, showing medium to high tree-pollen percentages, medium PCA1 values decreasing to low values, and an early maximum in PCA2 values. This reflects moist soils and local snow beds, well-developed in the early period.

The LGI/YD transitions show distinctly different features in each lake: In *Ristjønna* (see also Paus et al., 2011), the LGI/YD transition is characterized by: (1) No lithostratigraphical disturbances (Fig. 9); (2) gradual and smooth pollen curve patterns across the transition (Fig. 9); (3) continuous presence of aquatics; and (4) continuous deposition of stones at the lake bottom until the end of the YD. Most probably, the stones were brought by shore-ice to the lake-center and dropped during melting (Paus et al., 2006, 2011; cf. Zimmermann et al., 2011). Altogether, this shows that Ristjønna was an open lake during summers, and uncovered by glaciers in the period from the LGI to the YD.

In *Topptjønna* (see also Paus et al., 2011), the homogenous clay/silt shows no traces of disturbance at the biostratigraphical LGI/YD transition. This indicates a low-energetic depositional environment within the restricted catchment. However, abrupt changes in the pollen and aquatics at the transition point to a hiatus. We do not think that this reflects the formation of a YD glacier covering the lake. As Topptjønna is shallow and its catchment is flat, paraglacial processes would have eroded its LGI sediments. Instead, the hiatus probably

570 reflects the change from semi-permanent lake ice in the late LGI to perennial ice that blocked
571 deposition during the early YD cold period.
572
573 In arctic-alpine areas today, deeper lakes thaw slower than shallow lakes (Vincent et al., 2008;
574 Novikmec et al., 2013). Therefore, it seems contradictory that the large and deep Ristjønna
575 retained ice-free conditions during the YD summers, whereas the smaller and shallower
576 Topptjønna did not. However, in contrast to Ristjønna, Topptjønna is located at a windy
577 position in a saddle point (Fig. 1) that decreases snow cover during winter. Lakes with
578 shallow snow cover will develop thicker ice and have a later ice break-up date than similar
579 lakes with thinner ice (Vincent et al., 2008). Also, the higher altitude of Topptjønna delays
580 ice-free conditions (Novikmec et al., 2013). Hence, it is plausible that Ristjønna stayed ice-
581 free during summers in the YD, whereas a perennial ice cover developed at Topptjønna.
582
583 In *Finnsjøen*, the abrupt shift at 2191 cm depth, both biostratigraphically (paz F-1/F-2
584 transition; Fig. 3) and lithostratigraphically (Table 2, Fig. 8), reflects a hiatus that may span at
585 least 800-900 years (see section 5.1.). The stratified sand layers above 2191 cm depth show
586 disturbances within the catchment before a low-energy depositional environment established
587 as signalled by the weakly developed and fine-grained laminations (Fig. 7). We think the
588 hiatus reflects the development of a local perennial snow drift/ice cap that blocked sediment
589 deposition. When the ice started melting in the late YD, the sand layers were deposited.
590 Apparently, sediments below the ice were not eroded, similar to the interglacial deposits on
591 Baffin Island that escaped erosive action by over-riding glaciers (Briner et al., 2007). Our
592 interpretation is supported by the facts that: (1) the coring point is situated in a deep and
593 restricted depression that could avoid glacial erosion, (2) the coring point is situated close to a
594 steep hill with a NE aspect (Fig. 1) where snow melts late in the summers today, (3)

595 stratigraphies similar to that of Finnsjøen are not recognized in the adjacent Topptjønna or
596 Ristjønna (Fig. 9) underlining the local feature of the YD ice development.
597
598 *Flåfattjønna* (see also Paus et al., 2006) deviates from the other lakes by lacking period 2
599 (YD-PBO) thus reflecting a hiatus of at least 1500 years (12.85-11.3 cal ka BP). Above the
600 hiatus, a stratified sand/silt layer (Fig. 9) shows high-energy depositional environments within
601 the catchment similar to the Finnsjøen sand layers, reflecting the melting of the local YD ice.
602 Flåfattjønna is a deep lake in a small catchment (Table 1), so a cold-based none-erosive YD
603 glacier could have established here and blocked sedimentation. Probably, this glacier did not
604 compact the LGI sediments because the lake and catchment topography prevented water and
605 water-saturated sediments to escape. The hiatus spans a longer period than that of Finnsjøen,
606 which indicates that Flåfattjønna was covered by a larger glacier of more regional character.
607 This distinctly contrasts previous interpretations: that the Flåfattjønna hiatus reflects perennial
608 lake-ice during the YD (Paus et al., 2006) or during the YD-PBO period (Paus, 2010).
609
610 *5.4. Dovre glaciation dynamics (Fig. 10)*
611
612 In the Weichselian period, glacier margins in west- and mid-Norway withdrew towards east-
613 southeast during interstadials and advanced towards west-northwest during stadial periods
614 (e.g. Mangerud, 1991; Lambeck et al., 2010; Wohlfarth, 2010; Olsen et al., 2013). It is likely
615 that the deglaciation of the Dovre region in the pre-LGI period (Dahl et al., 1997; Paus et al.,
616 2006, 2011; Bøe et al., 2007; Goehring et al., 2008) followed a similar pattern. This could
617 explain why the eastern Flåfattjønna has more dominant tree pollen in the LGI than the
618 western lakes (Fig. 9). An eastern regional glacier close to Flåfattjønna would have severely

hampered the development of local vegetation and its pollen production, and reinforced the relative representation of long-distance tree pollen.

The mean surface exposure age (21.7±0.8 ka) from the summit of Mt. Rødalshø adjacent to Flåfattjønna (Fig. 1) could be argued to reflect the minimum age of ice-free conditions at the summit, but such an interpretation is unreasonable without supporting surface exposure ages from multiple nuclide or boulder-bedrock pairs. No erratics were investigated in this study, but data from further east show that summit erratics yield substantially lower ages than the bedrock they rest on (Goehring et al., 2008). Hence, the surface exposure ages obtained from the summit should be regarded as apparent ^{10}Be exposure ages only, without speculating whether they result from certain episodes of prior exposure.

The two lower elevation samples from the slopes of Rødalshø yield overlapping surface exposure ages (mean age 11.1±0.5 ka). These surfaces appear ice moulded and can be considered to show the timing of deglaciation. The lowermost sample location is more likely to have thicker/more long-lasting snow cover, hence the sample RØD-0304 (11.3±0.4 ka) is considered to be the more reliable of the two. Shielding by seasonal snow cover seems to be minor as the lower-elevation surface exposure ages overlap with the lowermost radiocarbon age from Flåfattjønna (11.2 cal ka BP; Paus, 2010). The lack of surface exposure ages from nearby erratic boulders can be compensated by data from a valley less than 25 km SW of Rødalshø. Here, a boulder-bedrock pair (1250 m a.s.l. at Einståkåskardet) gives 12.6±1.1 ka (n = 2) and an adjacent bedrock surface (1200 m a.s.l.) gives 12.2±0.4 ka (Linge unpublished data).

643 During the YD cooling, glaciers advanced from the east and covered Flåfattjønna (Fig. 10).
644 According to the Ristjønna and Topptjønna stratigraphy, a regional glacier did not reach the
645 mountain ridge where these lakes are situated, 30 km west of Flåfattjønna. Therefore, the
646 glacial lineations and moraines at high altitudes within this western region must be older than
647 the interpreted YD age (Follestad, 2005; Follestad and Fredin, 2007; Olsen et al., 2014).
648 However, local ice-caps/glaciers did develop here, as evidenced in the Finnsjøen deposits.
649
650 The Dovre glaciers may have started to advance prior to the YD (Fig. 10) as a parallel to the
651 late Allerød advances in western Norway (Lohne et al., 2007). Already in the last half of the
652 Allerød, a cold-temperature signal, i.e. the increase of pioneers, is found in the Topptjønna
653 and Ristjønna pollen diagrams (Paus et al., 2011). This is in line with the decreasing LGI
654 temperatures signalled in the Greenland ice-cores (Johnsen et al. 2001). Furthermore, pioneers
655 are sparsely represented below the hiati in the Flåfattjønna and Finnsjøen diagrams, which
656 may indicate that glaciers blocked sedimentation in these lakes before the regional cold signal
657 fully developed in the late Allerød. According to Olsen et al. (2013), the regional YD glacial
658 maximum is reflected by the Tautra morainic stage in late Allerød/early YD.
659
660 A similar YD readvance must have occurred elsewhere in the Scandes Mountains. For
661 example, megafossil ages and ^{10}Be surface exposure ages show that Mt. Åreskutan became
662 ice-free during the LGI (Kullman, 2008) but was ice-covered during the YD (Johnsen, 2010).
663 Megafossils can be preserved beneath glaciers for several thousands of years (Benedict et al.,
664 2008; Öberg and Kullman, 2011). Accordingly, the Åreskutan megafossils found in a snow
665 bed basin depressed in a small catchment, could very well have survived a YD reglaciation.
666

After the YD glacial maximum, the deglaciation in mid-Norway developed stepwise (Olsen et al., 2013, 2014). The local ice cap over Finnsjøen disappeared ca. 12 cal ka BP followed by an algae maximum in mid paz F-2, which points to milder temperatures (see section 5.2.2.). Consequently, increased temperatures, and not only lowered winter precipitation, could explain the YD glacier withdrawal. As deglaciation progressed, the eastern Flåfattjønna became ice-free around 11.3-11.2 cal ka BP (Fig. 10) according to AMS-dating of macrofossils from the Flåfattjønna deposits (Paus, 2010) and ^{10}Be surface exposure ages of bedrock surfaces (Table 4).

6. Conclusions

- The fossil pollen and DNA from our well-dated (AMS) laminated sediments in Lake Finnsjøen showed uninterrupted local vegetation development from late YD (ca 12 cal ka BP) to early Holocene around 9.7 cal ka BP. The earliest local vegetation in late YD/early Holocene was extremely sparse including snow-beds with *Beckwithia, Oxyria, Saxifraga* spp., and dwarf-willows, ridges with *Artemisia norvegica* and *Papaver*, and lee sides with *Betula nana*, grasses and *Selaginella*. From 11.3 cal ka BP, local vegetation rapidly closed with *Saxifraga* spp. and *Silene acaulis* in snow-beds and *Dryas* on ridges. From 10.7 cal ka BP, open birch-forests developed with juniper, *Empetrum* and other dwarf-shrubs. Pine forests established within the area from 10.3 cal ka BP.
- We identified the Pre Boreal Oscillation (PBO) around 11.4 cal ka BP by a tree-birch minimum and maxima in *Artemisia, Selaginella* and grasses. This signals the effect of decreased long-distance tree-birch pollen. Distinct local changes were not detected until the post-PBO warming. The earlier warming at the YD/Holocene transition at 11.65 cal ka BP was too weak and short-lived for vegetation closure at high altitudes at Dovre.

- A local ice cap covered Lake Finnsjøen during parts of the YD without removing older deposits causing a hiatus of at least 800-900 years, separating the late YD from Late-Glacial interstadial (LGI) sediments.
- Sediments from Finnsjøen and the three previously studied Dovre lakes tell four different LG histories: Ristjønna showed uninterrupted sediments indicating an open lake during summers from LGI to the early Holocene, Topptjønna was covered by permanent lake-ice during parts of YD, Finnsjøen was covered by a local YD ice-cap, and Flåfattjønna was covered by a regional glacier from late Allerød to the early Holocene.
- Parts of Dovre show two LG deglaciations: one in the pre-LGI and one in the late YD/early Holocene, involving a considerable YD reglaciation. This suggests that the most reasonable Scandinavian ice model is the one that is intermediate between the maximum ice model postulating a large glacier during the entire LG, and the minimum ice model postulating thin and multidomed early LG ice. This modified ice model also implies that the Åreskutan LGI megafossils could have been preserved beneath readvancing YD ice.
- We have demonstrated that hiati in deep lakes that avoided glacial erosion represent a new stratigraphical tool for identifying glacier advances/re-advances.
- As LG terrestrial macrofossils are lacking in all four Dovre lakes, the LG chronology is exclusively based on stratigraphical correlations and considerations. It has to be thoroughly tested by future studies providing reliable AMS-dates of terrestrial fossils.
-

Acknowledgements

716 Espen Paus, Erling Straalberg, and Ståle Samuelshaug helped during coring, Josef Kusior
717 modified the corer, Linn Cecilie Krüger prepared the pollen samples, Beate Helle drew figs.
718 1, 2, 5, and 9, Eva Bjørseth and Irene Heggstad helped with Figure 7, and Helitrans brought
719 us safely to Lake Finnsjøen. Mathias Trachsel helped modelling the age-depth relationships,
720 Maria Miguens-Rodriguez helped preparing rock samples for cosmogenic ^{10}Be analysis,
721 Sheng Xu performed the AMS measurements, and Audun Schrøder Nielsen helped with the
722 laboratory analyses of the sedaDNA samples. We thank all sincerely. We also want to thank
723 Karin Helmens and two anonymous reviewers for valuable comments significantly improving
724 the manuscript. AP wishes to honour his late father Stig who introduced him to Botany and
725 Quaternary Geology. The field-work and dating were supported by the Olaf Grolle-Olsen and
726 Meltzer University Foundations. The DNA analysis was supported by the Research Council
727 of Norway (grant no. 191627/V40 to CB).
728
729
730 **References**
731
732 Aario, L., 1940. Waldgrenzen und subrezente Pollenspektern in Petsamo Lappland. Annales
733 Acad. Scient. Fennica A 54 (8), 1-120.
734 Andersen, B.G., 1981. Late Weichselian ice sheets in Eurasia, Greenland and Norway. In:
735 Denton, G.H. and Hughes, T.J. (eds.): The last Great Ice Sheets, 20-27. Wiley, New York.
736 Arnold, N.S., van Andel, T.H., Valen, V., 2002. Extent and dynamics of the Scandinavian ice
737 sheet during Oxygen Isotope Stage 3 (65,000-25,000 BP). Quat. Res. 57, 38-48.
738 Bakke, J., Dahl, S.O., Nesje, A., 2005. Lateglacial and early Holocene palaeoclimatic
739 reconstruction based on glacier fluctuations and equilibrium-line altitudes at northern
740 Folgefonna, Hardanger, western Norway. J. Quat. Sci. 20, 179-198.

741 Balco, G., Stone, J.O., Lifton, N.A., Dunai, T.J., 2008. A complete and easily accessible
742 means of calculating surface exposure ages or erosion rates from ^{10}Be and ^{26}Al
743 measurements. Quat. Geochron. 3, 174-195.
744 Belzile, C., Vincent, W. F., Gibson, J. A. E., Van Hove, P., 2001. Bio-optical characteristics
745 of the snow, ice, and water column of a perennially ice-covered lake in the High Arctic.
746 Can. J. Fisheries Aq. Sci. 58, 2405-2418.
747 Benedict, J.B., Benedict, R.J., Lee, C.M., Staley, D.M., 2008. Spruce trees from a melting ice
748 patch: evidence for Holocene climatic change in the Colorado Rocky Mountains, USA.
749 The Holocene 18, 1067–1076.
750 Birks, H.H., Larsen, E., Birks, H.J.B., 2005. Did tree-Betula, Pinus and Picea survive the last
751 glaciation along the west coast of Norway? A review of the evidence, in light of
752 Kullman (2002). J. Biogeogr. 32, 1461–1471.
753 Birks, H.J.B., Line, J.M.L., 1992. The use of rarefaction analysis for estimating palynological
754 richness from Quaternary pollen-analytical data. The Holocene 2, 1-10.
755 Björck, S., Rundgren, M., Ingólfsson, Ó., Funder, S., 1997. The Preboreal oscillation around
756 the Nordic Seas: terrestrial and lacustrine responses. J. Quat. Sci. 12, 455-465.
757 Blaauw, M, Christen, J.A., 2011. Flexible paleoclimate age-depth models using an
758 autoregressive gamma process. Bayesian Analysis 6, 457-474.
759 Boessenkool, S., Mcglynn, G., Epp, L.S., Taylor, D., Pimentel, M., Gizaw, A., Nemomissa,
760 S., Brochmann, C., Popp, M., 2014. Use of Ancient Sedimentary DNA as a Novel
761 Conservation Tool for High-Altitude Tropical Biodiversity. Conserv. Biol. 28, 446-455.
762 Bøe, A.G., Murray, A., Dahl, S.O., 2007. Resetting of sediments mobilised by the LGM ice-
763 sheet in southern Norway. Quat. Geochron. 2, 222-228.
764 Bondevik, S., Mangerud, S., Gulliksen, S. 2001. The marine ^{14}C age of the Vedde Ash Bed
765 along the west coast of Norway. J. Quat. Sci.16, 3-7.

766 Brauer, A., Casanova, J., 2001. Chronology and depositional processes of the laminated
767 sediment record from Lac d'Annecy, French Alps. J. Paleolimn. 25, 163-177.
768 Briner, J.P., Axford, Y., Forman, S.L., Miller, G.H., Wolfe, A.P., 2007. Multiple generations
769 of interglacial sediments preserved beneath the Laurentide Ice Sheet. Geology 35, 887-
770 890.
771 Child, D., Elliott, G., Mifsud, C., Smith, A.M., Fink, D., 2000. Sample processing for earth
772 science studies at ANTARES. Nucl. Instrum. Meth. B 172, 856-860.
773 Coissac, E., 2012. OligoTag: a program for designing sets of tags for next-generation
774 sequencing of multiplexed samples. In: Pompanon, F., Bonin, A. (eds): Data Production
775 and Analysis in Population Genomics Humana Press, New York, pp. 13-31.
776 CRONUS-Earth, 2015: Online calculators: http://hess.ess.washington.edu/math/. Accessed
777 January 2015.
778 Cook, T.L., Bradley, S.R., 2010: An analysis of past and future changes in the ice cover of
779 two high-arctic lakes based on Synthetic Aperture Radar (SAR) and landsat imagery.
780 Arct. Antarct. Alp. Res. 42, 9-18.
781 Dahl, S.O., Nesje, A., Øvstedal, J., 1997. Cirque glaciers as morphological evidence for a thin
782 Younger Dryas ice sheet in the east-central southern Norway. Boreas 26, 161-180.
783 Davis, M.B., Moeller, R.E, Brubaker, L.B., 1984. Sediment focusing and pollen influx. In:
784 Haworth, E.Y, Lund, J.W.G. (eds.): Lake sediments and environmental history, 261-
785 293.University of Leicester, Leicester.
786 De Barba, M., Miquel, C., Boyer, F., Mercier, C., Rioux, D., Coissac, E., Taberlet, P., 2014.
787 DNA metabarcoding multiplexing and validation of data accuracy for diet assessment:
788 application to omnivorous diet. Molecular Ecol. Resources 14: 306-323.
789 Denton, G. H., Alley, R. B., Comer, G. C. & Broecker, W. S., 2005. The role of seasonality in
790 abrupt climate change. Quat. Sci. Rev. 24**,** 1159-1182.

791 DNMI, 2015. Det Norske Meteorologiske Institutt web pages:
792 http://met.no/Klima/Klimastatistikk/Klimadata/. Accessed January 2015.
793 Dunne, J., Elmore, D., Muzikar, P., 1999. Scaling factors for the rates of production of
794 cosmogenic nuclides for geometric shielding and attenuation at depth on sloped
795 surfaces. Geomorphology 27, 3-11.
796 Fægri, K., Iversen, J., 1989. Textbook of pollen analysis. 4. revised edition by Fægri, K.,
797 Kaland, P.E., Krzywinski, K. Wiley, Chichester. 314 pp.
798 Follestad, B., 2005. Large-scale patterns of glacial streaming flow deduced from satellite
799 imagery over Sør-Trøndelag, Norway. Norw. J. Geol. 85, 225-232.
800 Follestad, B., Fredin, O., 2007. Late Weichselian ice flow evolution in south-central Norway.
801 Norw. J. Geol. 87, 281-289.
802 Fredskild, B., 1973. Studies in the vegetational history of Greenland. Palaeobotanical
803 investigations of some Holocene lake and bog deposits. Medd. Grønl.198(4). 245 pp.
804 Giesecke, T., 2005. Holocene forest development in the central Scandes Mountains, Sweden.
805 Veg. Hist. Archaeobot. 14, 133-147.
806 Goehring, B.M., Brook, E.J., Linge, H., Raisbeck, G.M., Yiou, F., 2008. Beryllium-10
807 exposure ages of erratic boulders in southern Norway and implications for the history of
808 the Fennoscandian Ice Sheet. Quat. Sci. Rev. 27, 320-336.
809 Goehring, B.M., Lohne, Ø.S., Mangerud, J., Svendsen, J.-I., Gyllencreutz, R., Schaefer, J.,
810 Finkel, R., 2012. Late Glacial and Holocene 10Be production rates for western Norway.
811 J. Quat. Sci. 27, 544-544.
812 Gosse, J.C., Phillips, F.M., 2000. Terrestrial in situ cosmogenic nuclides: theory and
813 application. Quat. Sci. Rev. 20, 1475-1560.

814 Grönvold, K., Oskarsson, N., Johnsen, S.J., Clausen, H.B., Hammer, C.U., Bond, G., Bard,
815 E., 1995. Ash layers from Iceland in the Greenland GRIP ice core correlated with
816 oceanic and land sediments. Earth and Planetary Science Letters 135, 149–155.
817 Grytnes, J.A., 2003. Species richness patterns of vascular plants along seven altitudinal
818 transects in Norway. Ecography 26, 291-300.
819 Hafsten, U., 1963. A late-glacial profile from Lista. South-Norway. Grana Palyn. 4, 326-337.
820 Helle, M., Sønstegaard, E., Coope, R.G. and Rye, N., 1981. Early Weichselian peat at
821 Brumunddal, southeastern Norway. Boreas 10, 369-279.
822 Høeg, H.I., 1994. Pollenanalytiske undersøkelser i Hirkjølområdet. Aktuelt fra Skogforsk 5–
823 94, 21 pp.
824 Hoek, W.Z., Bos, J.A.A., 2007. Early Holocene climate oscillations – causes and
825 consequences. Quat. Sci. Rev. 26, 1901 – 1906.
826 Holtedahl, O., 1955. On the Norwegian Continental Terrace, primarily outside Møre-
827 Romsdal: its geomorphology and sediments. Årb. Univ. Bergen. Nat. vit. rk. 14. 209 pp.
828 Jensen, C., Vorren, K.D., Mørkved, B., 2007. Annual pollen accumulation rate (PAR) at the
829 boreal and alpine forest-line of north-western Norway, with special emphasis on Pinus
830 sylvestris and Betula pubescens. Rev. Palaeobot. Palynol. 144, 337–361.
831 Johnsen, S.J., Dahl-Jensen, D., Gundestrup, N., Steffensen, J.P., Clausen, H.B., Miller, H.,
832 Masson-Delmotte, V., Sveinbjörnsdottir, A.E., White, J., 2001. Oxygen isotope and
833 palaeotemperature records from six Greenland ice-core stations: Camp Century, Dye-3,
834 GRIP, GISP2, Renland and NorthGRIP. J. Quat. Sci. 16, 299–307.
835 Johnsen, T.F., 2010. Late Quaternary ice sheet history and dynamics in central and southern
836 Scandinavia. Dr. Thesis, Dept. Phys. Geogr. Quat. Geol., Stockholm.
837 Jørgensen, T., Haile, J., Möller, P., Andreev, A., Boessenkool, S., Rassmussen, M., Kienast,
838 F., Coissac, E., Taberlet, P., Brochmann, C., Bigelow, N.H., Andersen, K., Orlando, L.,

839 Gilbert, M.T.P., Willerslev, E., 2012. A comparative study of ancient sedimentary
840 DNA, pollen and macrofossils from permafrost sediments of northern Siberia reveals
841 long-term vegetational stability. Molecular Ecology 21, 1989-2003.
842 Kolstrup, E., 1979. Herbs as July temperature indicators for parts of the Pleniglacial and
843 Lateglacial in the Netherlands. Geol. Mijnbouw. 58, 377-380.
844 Krill, A.G., 1987. Berggrunnskart Snøhetta 15194 1:50000. Norges geologiske undersøkelse.
845 (Bedrock map Snøhetta 15194 1:50000. Geological survey of Norway).
846 Krüger, L.C., Paus, A., Svendsen, J.I. & Bjune, A., 2011. Lateglacial vegetation and palaeo-
847 environment in western Norway with emphasis on the Sunnmøre region. Boreas 40,
848 616–635.
849 Kullman, L., 2002. Boreal tree taxa in the central Scandes during the Late-Glacial:
850 implications for Late Quaternary forest history. J. Biogeogr. 29, 1117-1124.
851 Kullman, L., 2008. Early postglacial appearance of tree species in northern Scandinavia:
852 review and perspective. Quat. Sci. Rev. 27, 2467-2472.
853 Laaksonen, K., 1976. The dependence of mean air temperatures upon latitude and
854 altitude in Fennoscandia (1921-1950). Ann. Acad. Scient. Fenn. A3, 199, 1-19.
855 Lambeck, K., Smither, C., Ekman, M., 1998. Tests of glacial rebound models for
856 Fennoscandinavia based on instrumented sea- and lake-level records. Geophys. J. Int.
857 135, 375-387.
858 Lambeck, K., Purcell, A., Zhao, J., Svensson, N-O., 2010. The Scandinavian Ice Sheet: from
859 MIS 4 to the end of the Last Glacial Maximum. Boreas 39, 410–435.
860 Larsen, D. J., Gifford, H.M., Geirsdottir, Á., Ólafsdottir, S., 2012. Non-linear Holocene
861 climate evolution in the North Atlantic: a high-resolution, multi-proxy record of
862 glacier activity and environmental change from Hvítárvatn, central Iceland. Quat. Sci.
863 Rev. 39, 14-25.

Lie, Ø., Dahl, S. O., Murrey, A. and Nesje, A., 2004. A large-scale deglaciation in central southern Norway during Isotopic Stage 3 (45-30 kyr BP): evidence based on geomorphology, ^{14}C and OSL dates. Nordic Geological Winter Meeting, Uppsala, Sweden.

Linge, H., Brook, E.J., Nesje, A., Raisbeck, G.M, Yiou, F., Clark, H., 2006. In situ Be-10 exposure ages from southeastern Norway; implications for the geometry of the Weichselian Scandinavian ice sheet. Quat. Sci. Rev. 25, 1097-1109.

Lohne, Ø.S., Bondevik, S., Mangerud, J., Svendsen, J.I., 2007. Sea-level fluctuations imply that the Younger Dryas ice-sheet expansion in western Norway commenced during the Allerød. Quat. Sci. Rev. 26, 2128–2151.

Mangerud, J., 1991. The last ice age in Scandinavia. In: Andersen, B.G., Königsson, L.-K. (eds.): Late Quaternary in the Nordic Countries 150,000-15,000 B.P. Striae 34, pp.15-30.

Mangerud, J., 2004. Ice sheets limits in Norway and on the Norwegian continental shelf. In: Ehlers, J. and Gibbard, P.L. (eds.): Quaternary Glaciations – Extent and Chronology. Elsevier, 271-294.

Moore, P.D., Webb, J.A., Collinson, M.E., 1991. Pollen analysis. Blackwell Scientific Publications, Oxford.

Nesje, A., 1992. A piston corer for lacustrine and marine sediments. Arct. Alp. Res. 24, 257-259.

Nesje, A., Bakke, J., Brooks, S.J., Kaufman, D.S., Kihlberg, E., Trachsel, M, D'Andrea, W.J., Matthews, J.A., 2014. Late glacial and Holocene environmental changes inferred from sediments in Lake Myklevatnet, Nordfjord, western Norway. Veget. Hist. Archaeobot. 23, 229-248.

888 Nielsen, O., Wolff, F.C., 1989. Geologisk kart over Norge, berggrunnskart RØROS & SVEG
889 – 1:250000. Norges geologiske undersøkelse.
890 Novikmec, M., Svitok, M., Kočicky, D., Šporka, F., Bitušík, P., 2013. Surface Water
891 Temperature and Ice Cover of Tatra Mountains Lakes Depend on Altitude, Topographic
892 Shading, and Bathymetry. Arct. Antarct. Alp. Res. 45, 77–87.
893 Öberg, L., Kullman, L., 2011. Recent glacier recession – a new source of postglacial treeline
894 and climate history in the Swedish Scandes. Landscape Online 26, 1-38.
895 DOI:10.3097/LO.201126
896 Odland, A., 1996. Differences in the vertical distribution pattern of *Betula pubescens* in
897 Norway and its ecological significance. Paläoklimaforschung 20, 43-59. Fischer Verlag,
898 Stuttgart.
899 Ojala, A.E.K., Francus, P., Zolitschka, B., Besonen, M., Lamoreux, S.F., 2012.
900 Characteristics of sedimentary varve chronologies - A review. Quat. Sci. Rev. 43, 45-
901 60.
902 Olsen, L., Sveian, H., Bergstrøm. B., Ottesen, D., Rise, L., 2013. Quaternary glaciations and
903 their variations in Norway and on the Norwegian continental shelf. In: Olsen, L., Fredin,
904 O., Olesen, O. (eds.): Quaternary geology of Norway. Geol. Surv. Norw. Special Publ.
905 13, pp. 27-78
906 Olsen, L., Høgaas, F., Sveian, F., Follestad, B., Klug, M., 2014. The Younger Dryas ice
907 margin positions in the Oppdal-Trondheim area. Poster abstract in Proceedings of the
908 31st Nordic Geological Winter Meeting, 141. Lund, Sweden, January 8-10 2014.
909 Owren, G.B., 1984. The vegetation history of the Dovre Mountains; the development during
910 the last 9000 years (in Norwegian). M.Sc.thesis, Univ. of Trondheim, Norway. 71pp.

911 Paasche, O., Larsen, J., 2010. Changes in lake stratification and oxygen distribution
912 inferredfrom two contrasting records of magnetotactic bacteria and diatoms. J. Geoph.
913 Res. 115, G02012, 11pp.
914 Paus, A., 1995. The Late Weichselian and early Holocene tree-birch history in S.Norway and
915 the Bølling *Betula* time-lag in NW Europe. Rev. Palaeobot. Palynol. 85, 243-262.
916 Paus, A., 2010. Vegetation and environment of the Rødalen alpine area, Central Norway, with
917 emphasis on the early Holocene. Veg. Hist. Archaeobot 19, 29-51.
918 Paus, A., 2013. Human impact, soil erosion, and vegetation response lags to climate change:
919 challenges for the mid-Scandinavian pollen-based transfer-function temperature
920 reconstructions. Veg. Hist. Archaeobot 22, 269-284.
921 Paus, A., Svendsen, J.I., Matiouchkov, A., 2003. Late Weichselian (Valdaian) and Holocene
922 vegetation and environmental history of the northern Timan Ridge, European Arctic
923 Russia. Quat. Sci. Rev. 22, 2285-2302.
924 Paus, A., Velle, G., Larsen, L., Nesje, A., Lie, Ø., 2006. Late-glacial nunataks in central
925 Scandinavia: biostratigraphical evidence for ice thickness from Lake Flåfattjønna,
926 Tynset, Norway. Quat. Sci. Rev. 25, 1228-1246.
927 Paus, A., Velle, G., Berge, J., 2011. The Late-glacial and early Holocene vegetation and
928 environment in the Dovre mountains, central Norway, as signalled in two late-glacial
929 nunatak lakes. Quat. Sci. Rev. 30, 1780-1796.
930 Paus, A., Boessenkool, S., Brochmann, C., Haflidason, H., 2014. The Late Weichselian
931 deglaciation of central Scandes; new stratigraphical evidences from laminated lake
932 sediments at Dovre, central Norway. Lecture abstract in Proceedings of the 31st Nordic
933 Geological Winter Meeting, 142. Lund, Sweden, January 8-10 2014.
934 Perren, B.B, Bradley, R.S., Francus, P., 2003. Rapid lacustrine response to recent High
935 Arctic warming: A diatom record from Sawtooth Lake, Ellesmere Island, Nunavut.

936 Arct. Antarct. Alp. Res. 35, 271-278.
937 Punt, W. et al., 1976-1996. The Northwest European Pollen Flora (NEPF) Vol I (1976), Vol II
938 (1980), Vol III (1981), Vol IV (1984) Vol V (1988), Vol VI (1991), Vol VII (1996),
939 Elsevier, Amsterdam.
940 Rasmussen, S.O., Andersen, K.K., Svensson, A.M., Steffensen, J.P., Vinther, B.M., Clausen,
941 H.B., Siggaard-Andersen, M.-L., Johnsen, S.J., Larsen, L.B., Bigler, M., Röthlisberger,
942 R., Fischer, H., Goto-Azuma, K., Hansson, M.E., Ruth, U., 2006. A new Greenland ice
943 core chronology for the last glacial termination. Journal of Geophysical Research 111
944 (D6), D06102.
945 Rasmussen, S.O., Vinther, B.M., Clausen, H.B., Andersen, K.K., 2007. Early Holocene
946 climate oscillations recorded in three Greenland cores. Quat. Sci. Rev. 26, 1907-1914.
947 Reimer, P.J., Bard, E., Bayliss, A., Beck, J.W., Blackwell, P.G., Ramsey, C.B., Buck, C.E.,
948 Edwards, R.L., Friedrich, M., Grootes, P.M., Thomas P. Guilderson, Haflidason, H.,
949 Hajdas, I., Hatté, C., Heaton, T.J., Hoffmann, D.L., Hogg, A.G., Hughen, K.A., Kaiser,
950 K.F., Kromer, B., Manning, S.W., Niu, M., Reimer, R.W., Richards, D.A., Scott, E.M.,
951 Southon, J.R., Turney, C.S.M., van der Plicht, J., 2013. INTCAL13 and MARINE13
952 radiocarbon age calibration curves 0-50,000 years cal BP. Radiocarbon 55, 1869-1887.
953 Ritchie, J. C. and Lichti-Federovich, S., 1967. Pollen dispersal phenomena in Arctic-Subarctic
954 Canada. Rev. Palaeobot. Palyn. 3, 255-266.
955 Seppä, H., 1998. Postglacial trends in palynological richness in the northern Fennoscandian
956 tree-line area and their ecological interpretation. The Holocene 8, 43-53.
957 Seppä, H., Hicks, S., 2006. Integration of modern and past pollen accumulation rate (PAR)
958 records across the arctic tree-line: a method for more precise vegetation reconstructions.
959 Quat. Sci. Rev. 25, 1501–1516.

960 Simonsen, A., 1980. Vertical variations of Holocene pollen sedimentation at Ulvik,
961 Hardanger, SW-Norway (in Norwegian). AmS-Varia 8, 86 pp.
962 Sollid, J.L., Carlson, A.B., Torp, B., 1980. Trollheimen-Sunndalsfjella-Oppdal
963 kvartærgeologisk kart 1 : 100 000. Geogr.Inst., Univ. i Oslo.
964 Soininen, E.M., Gauthier, G., Bilodeau, F., Berteaux, D., Gielly, L., Taberlet, P., Gussarova,
965 G., Bellemain, E., Hassel, K., Stenøien, H.K., Epp, L., Schrøder-Nielsen, A.,
966 Brochmann, C., Yoccoz, N.G., 2014. (Highly overlapping winter diet in two sympatric
967 lemming species revealed by DNA metabarcoding. PloS ONE (accepted).
968 Sønstebø, J.H., Gielly, L., Brysting, A.K., Elven, R., Edwards, M., Haile, J., Willerslev, E.,
969 Coissac, E., Rioux, D., Sannier, J., Taberlet, P., Brochmann, C., 2010. Using next-
970 generation sequencing for molecular reconstruction of past Arctic vegetation and
971 climate. Molecular Ecology Resources 10, 1009-1018.
972 Stockmarr, J., 1971. Tablets with spores in absolute pollen analysis. Pollen et Spores 13, 615-
973 621.
974 Stuiver, M., Reimer, P.J., Reimer, R., 2014. CALIB Radiocarbon Calibration, Execute
975 Version 7.02. http://calib.qub.ac.uk/calib/ Accessed April 2014.
976 Taberlet, P., Coissac, E., Pompanon, F., Gielly, L., Miquel, C., Valentini, A., Vermat, T.,
977 Corthier, G., Brochmann, C., Willerslev. E., 2007. Power and limitations of the
978 chloroplast *trn*L (UAA) intron for plant DNA barcoding. Nucleic Acids Research
979 35**:**e14. DOI:10.1093/nar/gkl938.
980 Terasmäe, J., 1951. On the pollen morphology of *Betula nana.* Svensk Bot. Tidskr. 45, 358-
981 361.
982 ter Braak, C.J.F., Smilauer, P., 1997- 2002. CANOCO for Windows, version 4.5 Biometrics –
983 Plant Research International, Wageningen, the Netherlands.

984 Thomas, E. R., Wolff, E.W., Mulvaney, R., Steffensen, J.P., Johnsen, .S.J., Arrowsmith, C,
985 White, J.W.C., Vaughn, B., Popp, T., 2007: The 8.2 ka event from Greenland ice cores.
986 Quat. Sci. Rev. 26, 70–81.
987 Troels-Smith, J., 1955. Karakterisering av løse jordarter. Danm. Geol. Unders. IV. Række 3,
988 73 pp.
989 Velle, G., Larsen, J., Eide, W., Peglar, S., Birks, H.J.B., 2005. Holocene environmental
990 history and climate of Råtåsjøen, a low-alpine lake in central Norway. J. Paleolimn. 33,
991 129-153.
992 Vincent, W. F., MacIntyre, S., Spige, R. H., and Laurion, I., 2008. The physical limnology of
993 high-latitude lakes. In: Vincent, W. F., Laybourn-Parry, J. (eds.): Polar Lakes and
994 Rivers: Limnology of Arctic and Antarctic Aquatic Ecosystems. Oxford: Oxford
995 University Press, 65–81.
996 Vorren, T., 1977. Weichselian ice movement in South Norway and adjacent areas. Boreas 6,
997 247-257.
998 Xu, S., Dougans, A.B., Freeman, S.P.H.T., Schnabel, C. & Wilcken, K.M., 2010. Improved
999 Be-10 and Al-26 AMS with a 5 MV spectrometer. Nucl. Instruments Meth. B 268, 736-
1000 738.
1001 Young, N.E., Schaefer, J.M., Briner, J.P., Goehring, B.M., 2013. A ^{10}Be production rate
1002 calibration for the Arctic. J Quat. Sci. 28, 515-526.
1003 Willerslev, E., Hansen, A. J., Binladen, J., Brand, T. B., Gilbert, M. T. P., Shapiro, B., Bunce,
1004 M., Wiuf, C., Gilichinsky, D. A., Cooper. A., 2003. Diverse plant and animal genetic
1005 records from Holocene and Pleistocene sediments. Science 300, 791–795.
1006 Willerslev, E., Hansen, A.J., Poinar, H.N., 2004. Isolation of nucleic acids and cultures from
1007 fossil ice and permafrost. Trends in Ecology & Evolution 19**,** 141-147.

1008 Willerslev, E., Cooper, A., 2005. Ancient DNA. Proceedings of the Royal Society B:
1009 Biological Sciences 272, 3-16.
1010 Willerslev, E., Davison, J., Moora, M., Zobel, M., Coissac, E., Edwards, M.E., Lorenzen,
1011 E.D., Vestergard, M., Gussarova, G., Haile, J., Craine, J., Gielly, L., Boessenkool, S.,
1012 Epp, L.S., Pearman, P.B., Cheddadi. R,, Murray, D., Brathen, K.A., Yoccoz, N.,
1013 Binney, H., Cruaud, C., Wincker, P., Goslar, T., Alsos, I.G., Bellemain, E., Brysting,
1014 A.K., Elven, R., Sønstebø J.H., Murton, J., Sher, A., Rasmussen, M., Ronn, R..,
1015 Mourier, T., Cooper, A., Austin, J., Moller, P., Froese, D., Zazula, G., Pompanon, F.,
1016 Rioux, D., Niderkorn, V., Tikhonov, A., Savvinov, G., Roberts, R.G., MacPhee, R.D.E.,
1017 Gilbert, M.T.P., Kjaer, K.H., Orlando, L., Brochmann, C., Taberlet, P., 2014. Fifty
1018 thousand years of Arctic vegetation and megafaunal diet. *Nature* 506, 47-51.
1019 Wohlfarth, B., 2010. Ice-free conditions in Sweden during Marine Oxygen Isotope Stage 3?
1020 Boreas 39, 377–398.
1021 Zimmerman, S.R.H., Pearl, C., Hemming, S.R., Tamulonis, K., Hemming, N.G., Searle, S.Y.,
1022 2011. Freshwater control of ice-rafted debris in the last glacial period at Mono Lake,
1023 California, USA. Quat. Res. 76, 264–271.
1024 Zolitschka, B., 2007. Varved lake sediments. *In*: Elias, S.A. (ed.): Encyclopedia of Quaternary
1025 Science. Elsevier, Amsterdam, pp. 3105-3114.
1026
1027 **Figure and Table captions.**
1028
1029 Fig. 1: Maps showing the Dovre area (small centre map), and the location of the lakes Store
1030 Finnsjøen, Ristjønna, Topptjønna (left map) and Flåfattjønna (right map). The contour
1031 interval is 100 m and 40 m for the local maps to the left and to the right, respectively. Sites for

1032 the TCN samples RØD 0301, 0304, 0307, and 0308 are indicated by 1, 4, 7, and 8,
1033 respectively, on the map to the right.
1034
1035 Fig. 2: X-ray photography of the studied core section 1980-2195 cm below water surface,
1036 with increasing depth towards the left. See Table 2 and section 4.1. for sediment descriptions.
1037 The holes show where samples for sedaDNA were taken. The positions of Fig. 7 (2110-2174
1038 cm), Fig. 8 (2174-2195 cm) and calibrated ages are indicated. The minerogenic/organic
1039 sediment transition at 2088 cm depth, 11.3 cal ka BP, reflects the post-PBO warming. The
1040 core-diameter (110 mm) is exaggerated in relation to the core length (115 cm).
1041
1042 Fig. 3: Lake Store Finnsjøen pollen diagram from the basal sediments, including dates, pollen
1043 assemblage zones, loss-on-ignition (LOI)-estimates, palynological richness (PR) estimates
1044 $E(T_{124})$, and total pollen concentration and accumulation rate estimates. Shaded curves
1045 represent 10x exaggeration of the scale. Note the change of depth scale at 2080 cm depth.
1046 Lithostratigraphical symbols follow Troels-Smith (1955) where diamond-shaped squares
1047 denote organic sediment content, whereas L-shaped symbols and dots denote minerogenic
1048 content (silt/clay and sand, respectively) in sediments. Asterisks (*) denote assumed ages
1049 discussed in sections 5.1. , 5.2. and used in estimating sedimentation rate and PAR.
1050
1051 Fig. 4: Plot of pollen taxa along the first two axes of the PCA on the merged pollen data from
1052 the four lakes, as displayed in Fig. 9. Eigenvalues: axis 1: 0.297, axis 2: 0.180, axis 3: 0.099,
1053 axis 4: 0.054. See section 4.2 for the ecological interpretations of the figure.
1054
1055 Fig. 5: The “Bacon” bayesian age-depth model (Blaauw and Christen, 2011) of the Finnsjøen
1056 core, overlaying the calibrated distributions of the seven individual dates. Grey-dotted lines

indicate the model's 95% probability intervals. Highest probability sedimentation is shown by the white line. It intersects the position of the paz-2/paz-3 transition (white square) which strongly suggests that the transition represents the onset of the Holocene, 11 650 cal yrs BP. Post (grey-shaded) and prior (single line) distributions of memory and accumulation rate, in addition to iteration features (Log of Objective) are included in the upper part.

Fig. 6. Photographs of sample locations for ^{10}Be surface exposure dating. (A) Sample RØD 0301 originates from a quartz lens (hammer for scale) at a vegetation-free and wind-exposed site. The bedrock surface appears to be both ice-moulded and weathered, causing the quartz lenses to protrude up to a few centimetres above the bedrock surface. Boulders of local bedrock are scattered around. (B) Sample RØD 0304 was collected from a quartz lens (plastic cup for scale) on an exposed surface surrounded by a cover of lichen-dominated dwarf-shrub heath. (C) Sample RØD 0307 originates from a quartz vein (circled) in bedrock, from a very exposed location near the summit of Rødalshø. The summit area appears to be stripped or plucked, as there is no material other than the occasional glacially transported boulder (local lithology and erratics). (D) Sample RØD 0308 originates from a quartz lens at the summit of Rødalshø (notebook for scale). Debris is confined to small depression, however, the cairn building might have cleaned the surface substantially.

Fig. 7: X-ray photography of the laminated silty clay at depth 2110-2174 cm with increasing depth towards the left. The downwards hammering of the core tube caused bending of laminations according to variations in sediment softness and viscosity.

Fig. 8: The basal sediments (2174-2195 cm depth) including the basal LGI silty clay gyttja (2191-2195 cm depth). Depth increases towards the left. The hole in the sand layer to the left

shows where sedaDNA was sampled. At 2191 cm depth, ca 1 cm to the left of /below the sedaDNA sampling point, the distinct transition between the light and ca 5 mm thick clay horizon below and the darker sand layer above, reflects the hiatus separating the LGI from the late YD.

Fig. 9: Lithostratigraphy (photos) and biostratigraphy (PCA, total pollen diagram) of the Dovre lakes Flåfattjønna (Paus et al. 2006), Finnsjøen (this study), and Topptjønna and Ristjønna (Paus et al. 2011). The dark lines separate the correlated periods 1 (pre-YD), 2 (from YD to end of PBO), and 3 (the early Holocene after PBO). The white horizontal lines show the onset of the Holocene. Note that period 2 is absent in the Flåfattjønna sediments.

Fig. 10: The summarized LG and early Holocene glacier and vegetation dynamics at Dovre as compiled from this study, Paus et al. (2006, 2011), and Paus (2010). Note that no datable LG macrofossils have been found in any of the four lakes, so the chronology earlier than 11.3 ka cal BP in each lake (dotted lines) is exclusively based on biostratigraphical and lithostratigraphical correlations and considerations. The tentative ages of the pre-LGI deglaciation are discussed in Paus et al. (2006, 2011).

Table 1: The features of the four Dovre lakes discussed in this study.

Table 2: The Finnsjøen lake sediment lithology from the core section studied.

Table 3: Results of the seven ^{14}C-dates from Finnsjøen. Calibrated ages (Stuiver et al., 2014) show probabilities within two sigma.

Table 4: Summary of ^{10}Be sample information for rock samples from Rødalen.

Part A: Summary of field data required for calculating surface exposure ages.

Part B: Laboratory data required for calculating ^{10}Be surface exposure ages and resulting age estimates.

Table 5: Names, dates, and biostratigraphical features of the local pollen assemblage zones. The rationale for the assumed ages denoted by asterisks (*), is given in Fig. 5 and section 5.1.

Table 6: Taxa identified by sedaDNA analyses of the Finnsjøen sediments. Laboratory sample names refer to coring points (3, 4), coring point sections (B, C), core depth, and laboratory numbering in brackets. The depth (cm) refers to depth below water surface correlated with coring point 4 from which pollen were analysed (Fig. 3). The ages (cal ka BP) of the pollen assemblage zones (paz) are noted. Taxa are ordered alphabetically.

Table 1

Table 1

Lake	Altitude m a.s.l.	Geogr. position	Basin size (m) - area (ha)	Max water depth (m)	Catchment size incl. basin (ha)	No of inlets and outlets
Store Finnsjøen	1260	62°24'N, 9°41'E	800 x 390 - 23.7	14.7	69	0 + 1
Ristjønna	1254	62°28'N, 9°37'E	1250 x 1000 - 68	12.1	275	1 +1
Topptjønna	1316	62°23'N, 9°40'E	200 x 300 - 4.2	6.9	45	0 + 1
Flåfattjønna	1110	62°20'N, 10°24'E	425 x 225 - 6	13	25	0 + 1

Table 2

Depth (cm)	**Description (Troels-Smith 1955)**	**Colour**	**Comments**
1980-2021	Ld^3 4, Dh +, Tb +, Ag +	Dark brown (nig 3)	Laminated gyttja with macro remains
2021-2050	Ld^2 2, Dh 1, Ag 1, As +	Brown (nig. 2+)	Laminated clay/silt gyttja. Includes several dark (nig 3) macrofossil-layers less than 1 cm thick. Most distinct between 2021 and 2023 cm ($Ld^2$1, Tb1, Dh1, Ag+). Two mm thick and light (nig 1) clay layer at 2026 cm depth.
2050-2063	$Ld^1$1, Ag 1, As 2	Grey brown (nig2-)	Laminated clay/silt gyttja. Thin macrofossil layers (nig 3), 3 between 2050-2054.5 cm and 2 between 2061-2063.
2063-2076	Ld^0 1, Ag 1, As 2	Brownish grey (nig2-)	Laminated clay/silt gyttja.
2076-2080	Ld^0 1, Ag 1, As 2	Grey brown (nig2)	Laminated clay/silt gyttja. Includes four distinct macrofossil layers (nig 3-). More silty in the upper part.
2080-2087.5	Ld^0 1, Ag 1, As 2	Grey brown (nig2)	Laminated clay/silt gyttja. Lighter in the upper part.
2087.5-2115	Ag 1, As 3	Grey (nig 2-)	Silty clay. Transition to the upper organic sediments clear cut. Shade of darker laminations between 2110-2115 cm.
2115-2173	Ag 1-, As 3+	Grey (nig 2-)	Laminated silty clay. Gradual and indistinct transition to the upper layer.
2173-2178	As 4, Ag +	Grey (nig 1+)	Laminated clay
2178-2180	Ag 2, As 1, Ga 1	Grey (nig 2+)	Sandy silt. Undulating upper and lower transitions
2180-2185	Ag 1, As 3,	Grey brown (nig 2-)	Silty clay. With fine laminations. Undulating upper transition.
2185-2191	Ag 1, Ga 3	Blue grey (nig 3+)	Two sand lenses divided by silty clay (As 3, Ag 1) at 2186.5-2187 cm
2191-2195	Ag 1, As 3, Ld^0+	Grey brown (nig 3-)	Laminated silty clay gyttja. At the upper transition, a 5 mm grey (nig 1) clay horizon occur.

Table 3

Lab.ref.	Depth (cm)	Age (year BP) Uncalibr.	Calibrated (2 ζ)	$\delta^{13}C$	Material dated (and its paz position)
TRa-4468	1994.5-1995.5	8845 ± 70	9683 - 10182	-27.0	Seeds of *Betula* undiff. and *B pubescens. B. nana* catkinscales. Bark, twigs and leaf remains. 16.1 mg. (paz F-6)
TRa-4469	2009-2010	8925 ± 65	9787 - 9848 (0.042) 9864 - 9877 (0.009) 9884 - 10227 (0.948)	-26.4	Leaf of *Salix polaris*. *Salix* budscales. Twigs and leaf remains. 17 mg. (paz F-6)
TRa-4471	2036.5-2038	9380 ± 115	10258 - 10875 (0.902) 10944 - 11076 (0.098)	-27.0	Leaves of *Dryas, Betula nana, Empetrum, Salix polaris, Salix* spp. *B.nana* catkin scales, *Salix* bud scales. Twigs. 33 mg. (paz F-5)
TRa-4472	2053.5-2055	9620 ± 85	10723 - 11200	-28.5	Leaves of *Dryas, Saxifraga oppositifolia, Betula nana, Empetrum*. Leaf stalks. 26.3 mg. (paz F-5)
ETH-48539	2062.5-2063	9557 ± 34	10725 - 10895 (0.465) 10918 - 11088 (0.535)	-28.2	*Dryas* leaves and seeds. *Salix* cupula. Remains of twigs, stems and leaves. 39.4 mg. (paz F-5)
ETH-48540	2079 - 2080	9743 ± 34	11130 - 11234	-26.8	Leaves of *Dryas, Saxifraga oppositifolia. Salix* bud scales. 49.6 mg. (early paz F-5)
Ua-45187	2085.5-2087.5	9908 ± 117	11104 - 11826 (0.991) 11890 - 11931 (0.009)	-25.8	Leaves of *Salix polaris, Saxifraga oppositifolia*. *Saxifraga* seeds. *Salix* bud scale. 3.7 mg. (paz F-4)

Table 4

Table 4A

Summary of field data required for calculation surface exposure ages.

Sample [a]	Elevation (m a.s.l.)	Surface type	Lithology	Latitude (°N)	Longitude (°E)	Shielding factor [b]	Thickness [c] (cm) (factor)
RØD-0301	1150	lens in bedrock	quartz in mica schist	62.326523	10.380965	0.9986	5.0 (0.9597)
RØD-0304	1060	lens in bedrock	quartz in mica schist	62.319778	10.353989	0.9970	4.0 (0.9676)
RØD-0307	1435	vein in bedrock	quartz in mica schist	62.315045	10.384162	1.0000	12.0 (0.9069)
RØD-0308	1438	lens in bedrock	quartz in mica schist	62.315045	10.384162	1.0000	7.0 (0.9442)

Table 4B

Laboratory data required for calculating ^{10}Be surface exposure ages and resulting age estimates.

Sample [a]	Quartz [d] (g)	Be carrier [e] (g)	^{10}Be/^{9}Be [f,g] ($\times 10^{-15}$)	^{10}Be conc. [g,h,i] (10^4 at g^{-1} SiO_2)	^{10}Be age [g,j,m] (ka)	^{10}Be age [g,k,m] (ka)	^{10}Be age [g,l,m] (ka)
RØD-0301	25.542	0.8287	227.0±6.68	14.41±0.53	10.13±0.94 (0.38)	10.92±0.59 (0.40)	11.29±0.60 (0.42)
RØD-0304	25.012	0.8205	202.0±7.65	12.93±0.58	9.74±0.93 (0.44)	10.49±0.63 (0.47)	10.85±0.64 (0.48)
RØD-0307	23.340	0.8181	473.0±14.0	32.80±1.19	19.35±1.78 (0.70)	20.85±1.12 (0.76)	21.56±1.14 (0.79)
RØD-0308	25.719	0.8270	545.7±15.3	34.76±1.21	19.66±1.80 (0.69)	21.19±1.12 (0.74)	21.91±1.14 (0.77)

[a] All samples processed and measured at SUERC. [b] Geometric shielding correction factor was computed after Dunne et al. (1999). [c] Sample thickness measured in cm from the surface, correction factor calculated assuming an exponential reduction in ^{10}Be production rate with depth (Gosse and Phillips 2000; Balco et al. 2008). [d] All samples use a density value of 2.65 g cm^{-3}. [e] Be carrier concentration: 299 µg g-1. [f] Isotope ratios normalized to the NIST SRM 4325 ^{10}Be standard with a nominal value of ^{10}Be/^{9}Be=3.06×10^{-11}. [g] Uncertainties are reported at the 1σ confidence level. [h] Procedural blank ^{10}Be/^{9}Be ratio of $4.66\pm0.90 \times 10^{-15}$ used to correct for background. [i] Propagated uncertainties include error in the blank and counting statistics. [j] Ages calculated using the Lm scaling scheme and the global reference ^{10}Be production rate of Balco et al. (2008). Propagated errors in the calculated ages include uncertainties of the ^{10}Be production rate and of the ^{10}Be decay constant. [k] Ages calculated using the Lm scaling scheme and the western Norway reference ^{10}Be production rate of Goehring et al. (2012). Propagated errors in the calculated ages include uncertainties of the ^{10}Be production rate and of the ^{10}Be decay constant. [l] Ages calculated using the Lm scaling scheme and the Arctic reference ^{10}Be production rate of Young et al. (2013). Propagated errors in the calculated ages include uncertainties of the ^{10}Be production rate and of the ^{10}Be decay constant. [m] ^{10}Be surface exposure ages were calculated using the CRONUS-Earth online calculator (Balco et al. 2008) version 2.2, assuming no atmospheric pressure anomalies (std model), no significant denudation during exposure (ε=0 mm a^{-1}), no prior exposure, and no temporal shielding (snow, sediment, vegetation). Errors in parenthesis are analytical errors only.

Table 5

Table 5.

PAZ (depths in cm)	Name	Age (cal. BP)	Pollen zone characteristics	Diagnostic taxa not included in Fig.3
F-6 (1980-2010)	*Pinus-Ulmus*	9700-10,300	Pine reaches 65 % ΣP whereas shrubs and herbs distinctly decrease. Total pollen concentration (TPC) and total PAR reach 35 10^4 grains cm^{-3} and 12 10^3 grains cm^{-2} a^{-1}, respectively. Palynological richness (PR) shows a strong decrease.	*Campanula* cf. *uniflora, Humulus, Melampyrum, Myricaria, Ranunculus acris-type, Sorbus, Ulmus*
F-5 (2010-2088)	*Salix-Dryas-Saxifraga*	10,300-11,300	In F-5a, *Artemisia*, Poaceae, and *Selaginella* distinctly decrease, and *Salix, Dryas, Silene* cf. *acaulis*, *Saxifraga oppositifolia*-type, and algae rapidly rise at the zone transition. In F5-b, *Betula*, *Juniperus*, *Empetrum*, and *Vaccinium*-type rise when *Dryas*, *Silene*, and *Saxifraga* decrease and *Corylus* becomes continuously represented. PR distinctly decreases. TPC rapidly rises from 10^3 to 10^5 grains cm^{-3}. Total PAR increases trough the zone: 4 - 30 10^2 grains cm^{-2} a^{-1}.	*Arctous alpinus, Astragalus/Oxytropis-type, Ephedra distachya*-type, *Hippophaë, Myricaria, Sorbus, Veronica, Ulmus*
F-4 (2088-2101)	*Populus-Artemisia*-Poaceae	11,300-*11,470	*Artemisia*, Poaceae, and *Selaginella* show local maxima, whereas *Betula* abruptly decreases. *Populus* is distinctly present. PR shows a weak maximum. TPC slightly decreases to 500-1000 grains cm^{-2} a^{-1}. Estimated tentative total PAR is 40-70 grains cm^{-2} a^{-1}.	*Arctostaphylos uva-ursi*,
F-3 (2101-2115)	*Betula-Populus-Rumex*	*11,470-*11,650	*Betula* and *Rumex* rapidly rise, whereas *Artemisia*, *Beckwithia*, Poaceae, and *Selaginella* abruptly decrease. *Populus* shows almost continuous representation. PR slightly decrease. TPC reaches max of 900-1400 grains cm^{-3}. Estimated tentative total PAR is 80-100 grains cm^{-2} a^{-1}.	*Anemone*-type, *Campanula* cf. *uniflora, Ephedra fragilis*-type, *Fagopyrum, Rhinanthus*
F-2 (2115-2191)	*Artemisia-Beckwithia* -Poaceae	*11,650-ca. *12,000	*Artemisia*, *Beckwithia*, Poaceae, *Selaginella*, other pioneers, and PR show maximum values; tree-pollen and algae reach low values. TPC decreases to max 800 grains cm^{-3}.	*Anemone*-type, *Campanula* cf. *uniflora, Ephedra distachya*-type, *Ephedra fragilis*-type, *Koenigia, Plantago lanceolata, Sagina*,
F-1 (2191-2195)	*Alnus-Betula-Pinus*	* > 12,850	*Pinus, Alnus* and algae show distinct maxima, whereas palynological richness (PR) and pioneers show minimum values. Total pollen concentration (TPC) reaches 10^4 grains cm^{-3}.	*Anemone*-type, *Arctous alpinus, Astragalus/Oxytropis-type, Campanula* cf. *uniflora, Hippophaë, Hippuris, Parnassia, Pedicularis, Sorbus, Ulmus*

Table 6

Table 6.

Laboratory sample name	Depth (cm)	Paz and ages (cal ka BP)	Taxon (no. of reads)
F4B_1980__2(SL171)	1980	F-6 (9.7-10.3)	*Alchemilla* sp. (93924) *Bartsia alpina* (23200) *Dryas octopetala* (60241) *Lycopodium* sp./*Diphasiastrum* sp. (4723) Salicaceae (118626)
F3B_1940__6(SL181)	1995-2000	F-6 (9.7-10.3)	*Dryas octopetala* (151364) Salicaceae (207524)
F4B_2000__1(SL158)	2000	F-6 (9.7-10.3)	*Quercus* sp. (80059) Salicaceae (123073)
F4C_2040__7(SL157)	2040	F-5b (10.3-10.7)	Arbutoideae (14167) *Bartsia alpina* (18329) *Bistorta vivipara* (29035) *Dryas octopetala* (74584) Salicaceae (151825) *Splachnum* sp. (579) *Pinus sylvestris* (19314)
F4C_2060__6(SL0168)	2060	F-5a (10.7-11.3)	*Dryas octopetala* (331584) *Equisetum* sp. (1390) Salicaceae (198024)
F4C_2080__5(SL156)	2080	F-5a (10.7-11.3)	Fagaceae (15914) Salicaceae (20660) *Saxifraga* sp. (79756)
F3B_2020__3(SL178)	2130	F-2 (11.65-12)	Asteraceae (271470)
F4C_2160__2(SL165)	2160	F-2 (11.65-12)	Asteraceae (138343)

Figure 1

Click here to download high resolution image

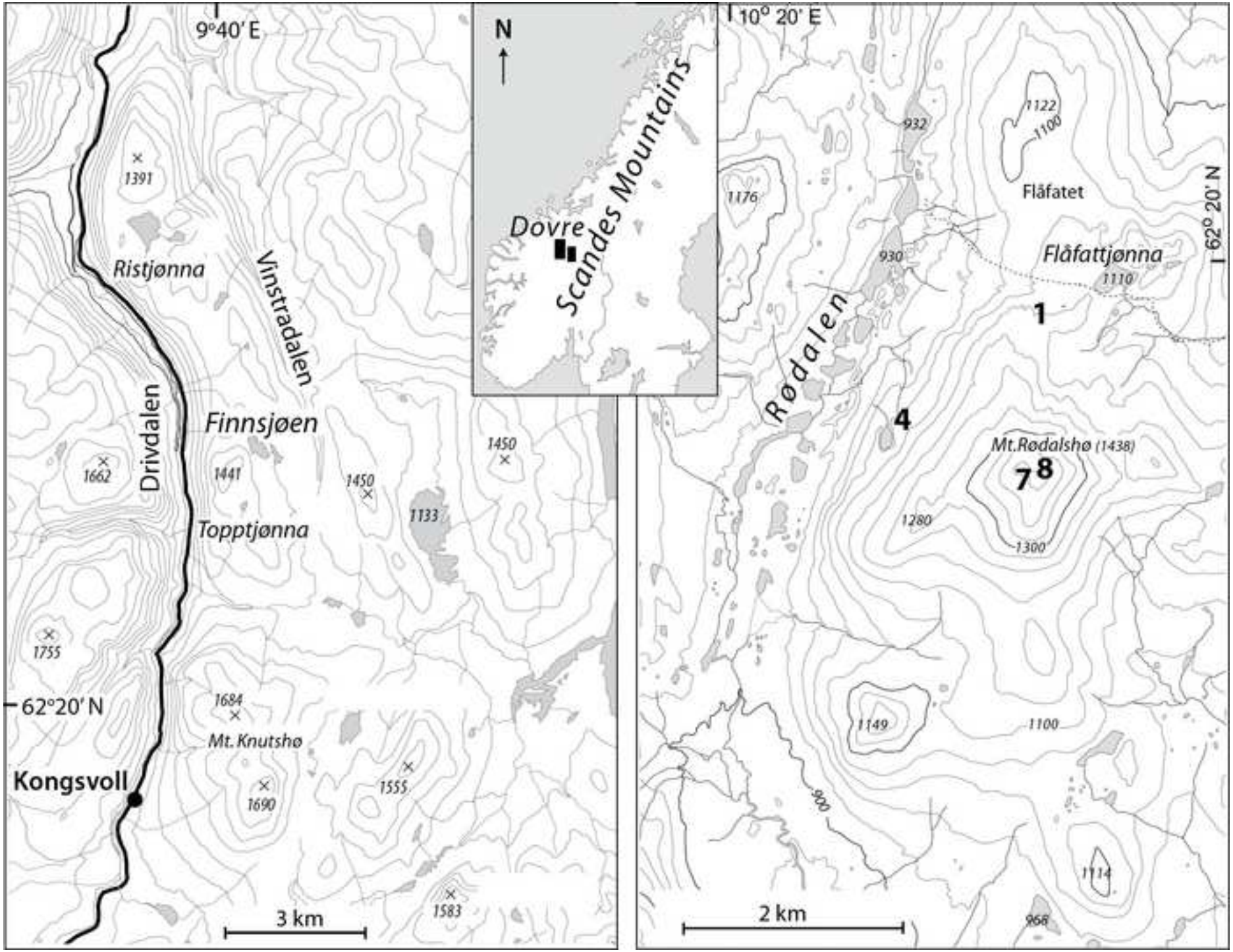

Figure 2

Click here to download high resolution image

Figure 3. Colour

Click here to download high resolution image

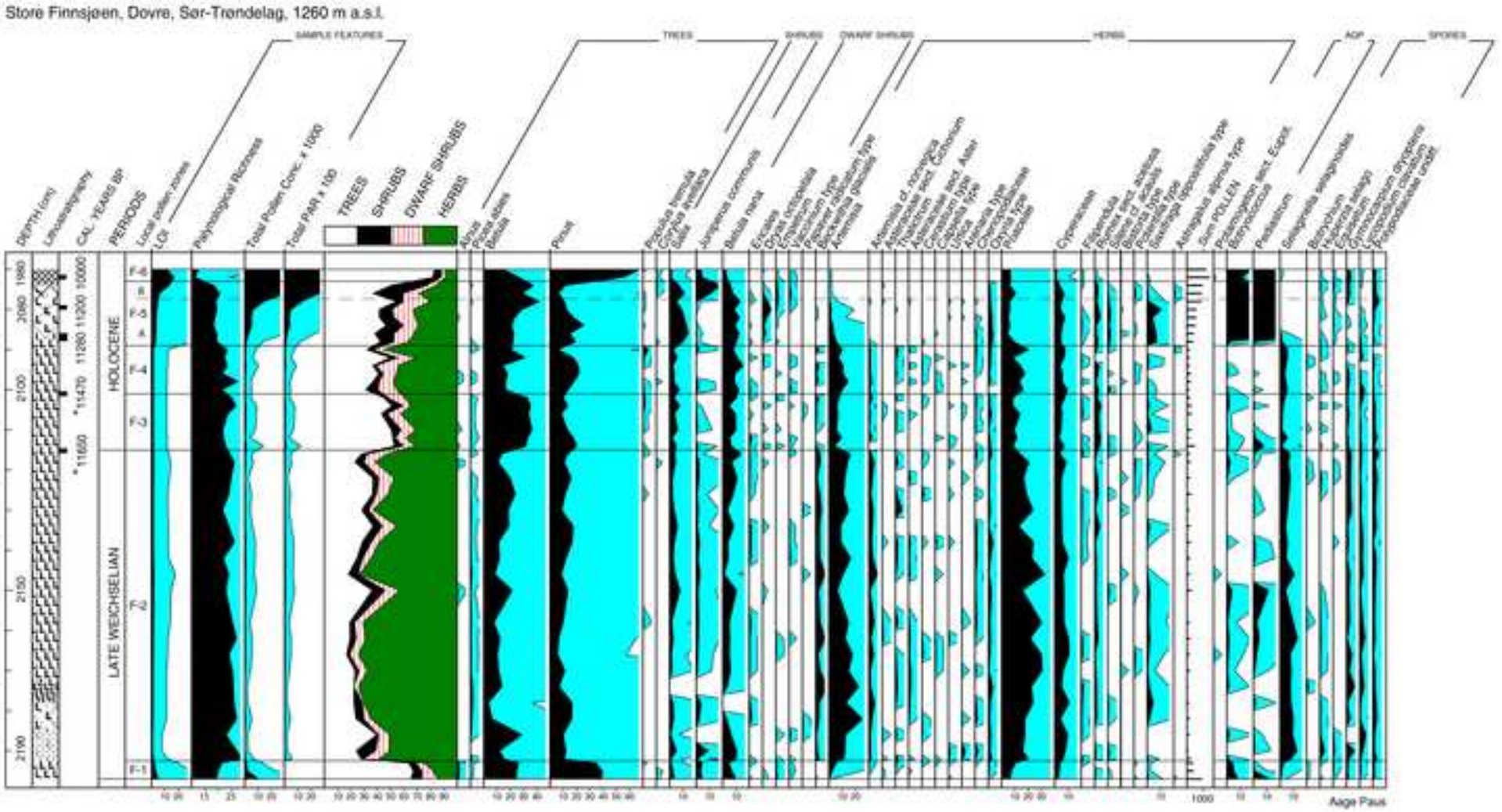

Figure 3. BW

Click here to download high resolution image

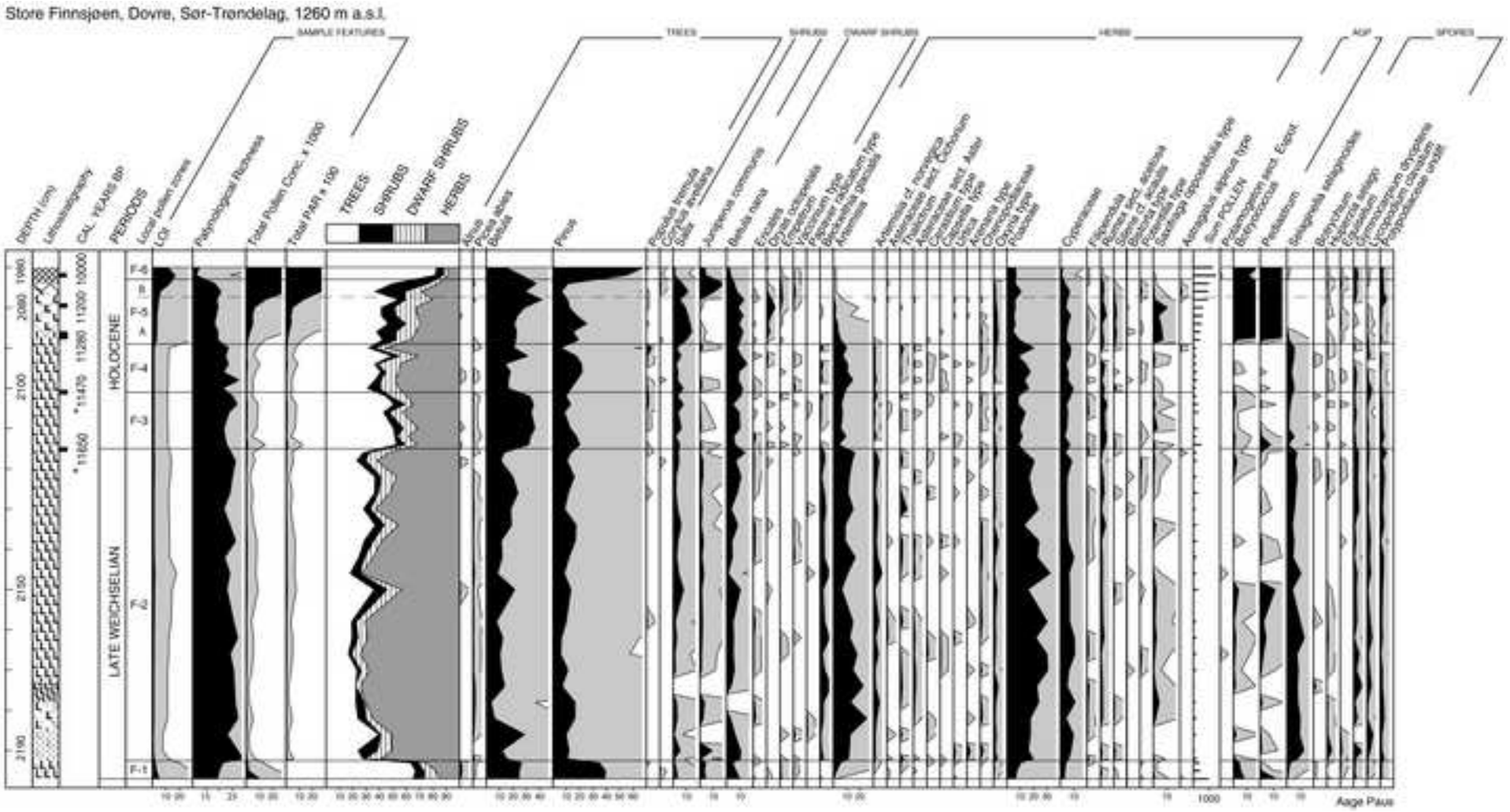

Figure 4

Click here to download high resolution image

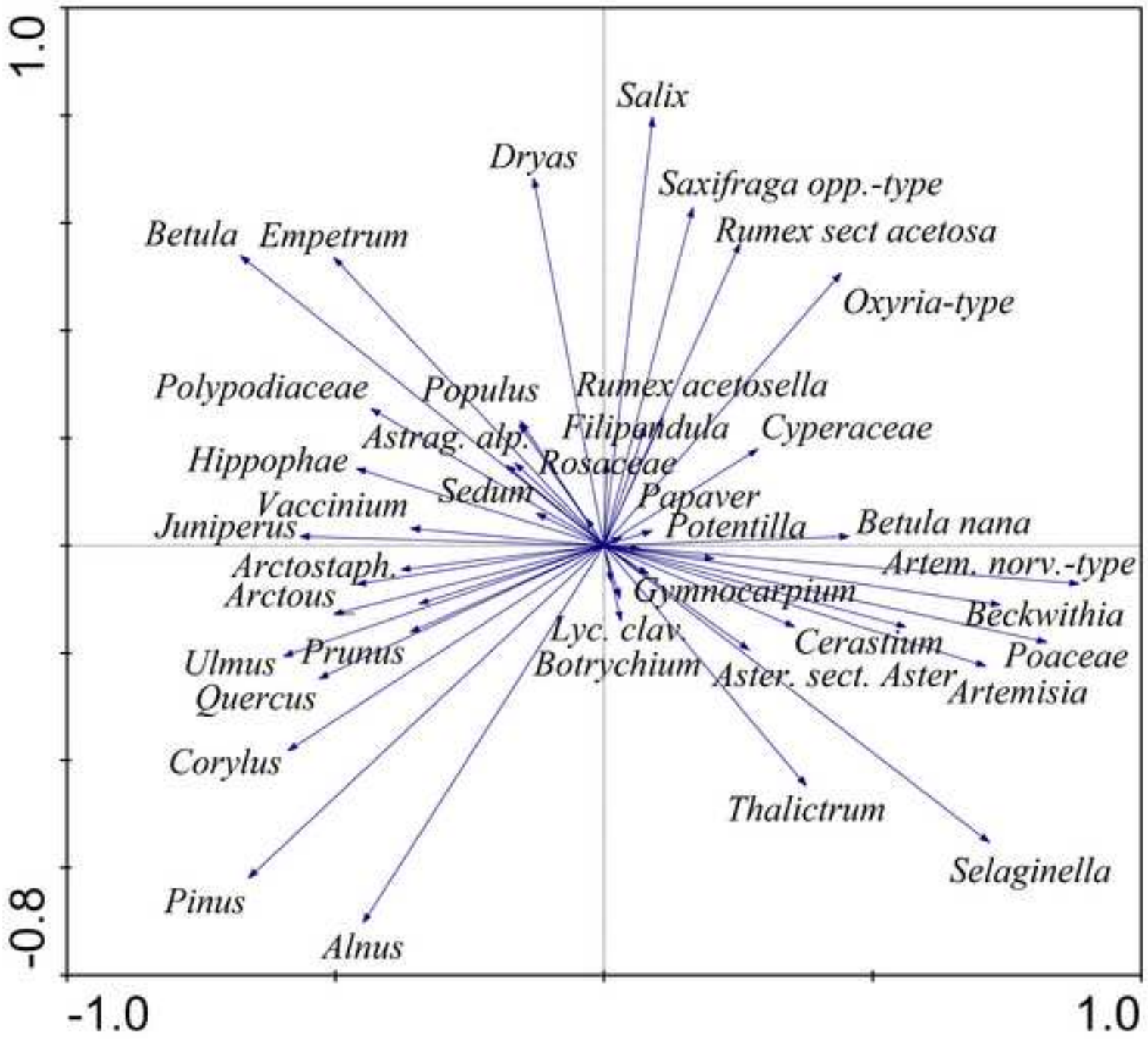

Figure 5

Click here to download high resolution image

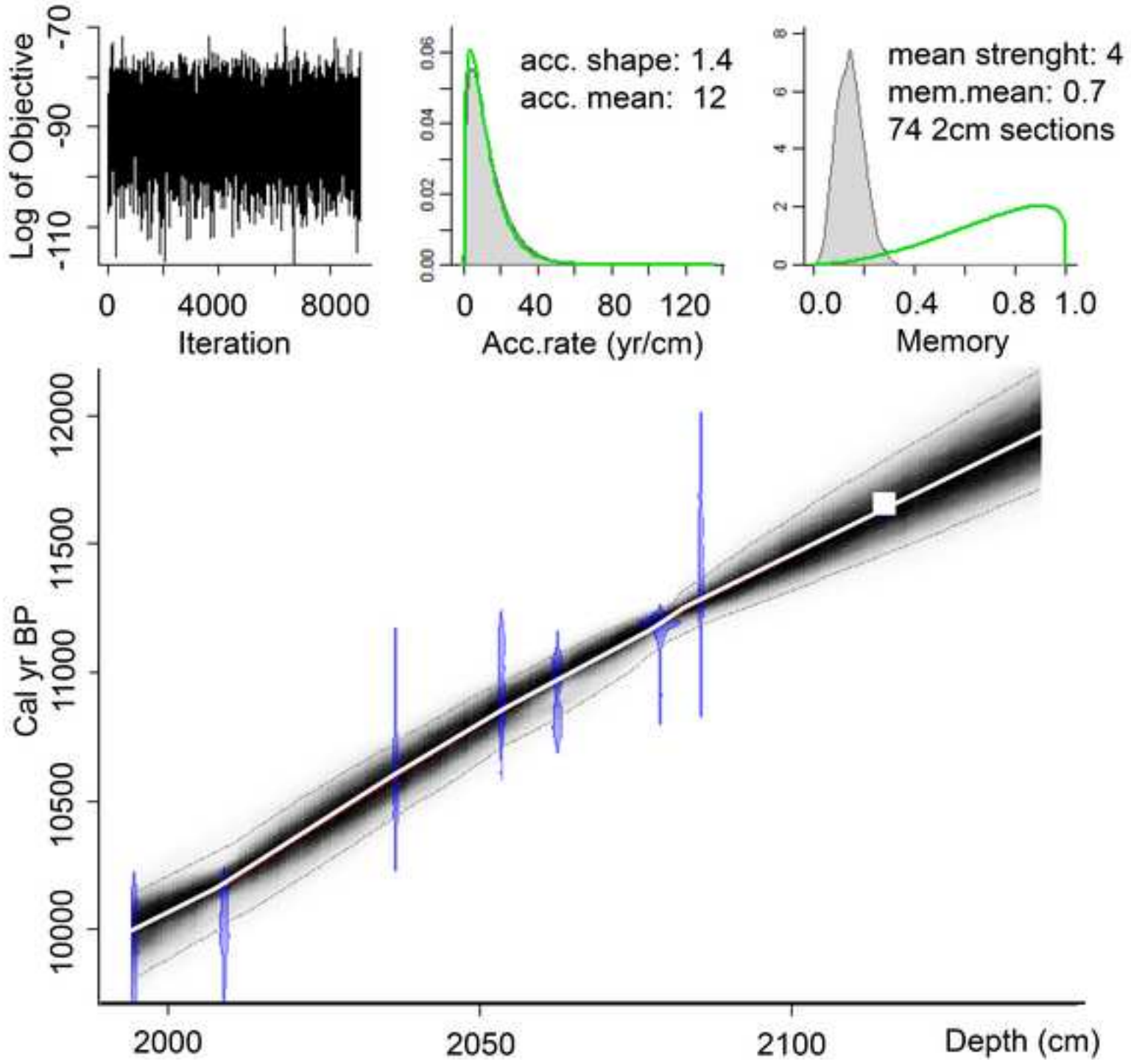

Figure 6. Colour

Click here to download high resolution image

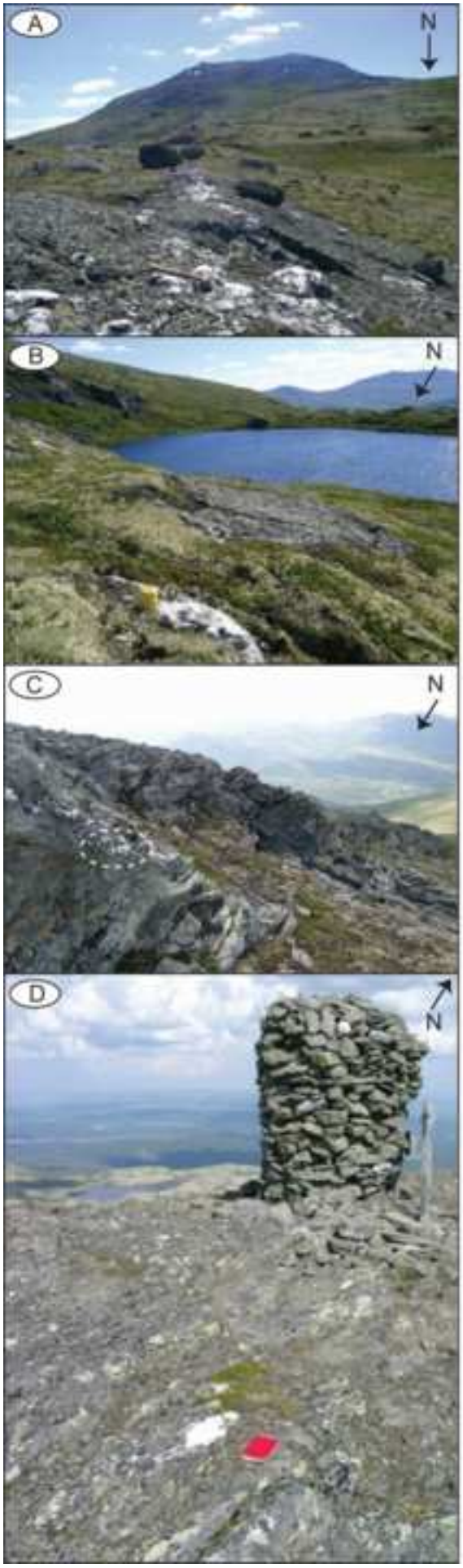

Figure 6. BW

Click here to download high resolution image

Figure 7

Click here to download high resolution image

Figure 8

Click here to download high resolution image

Figure 9. Colour

Click here to download high resolution image

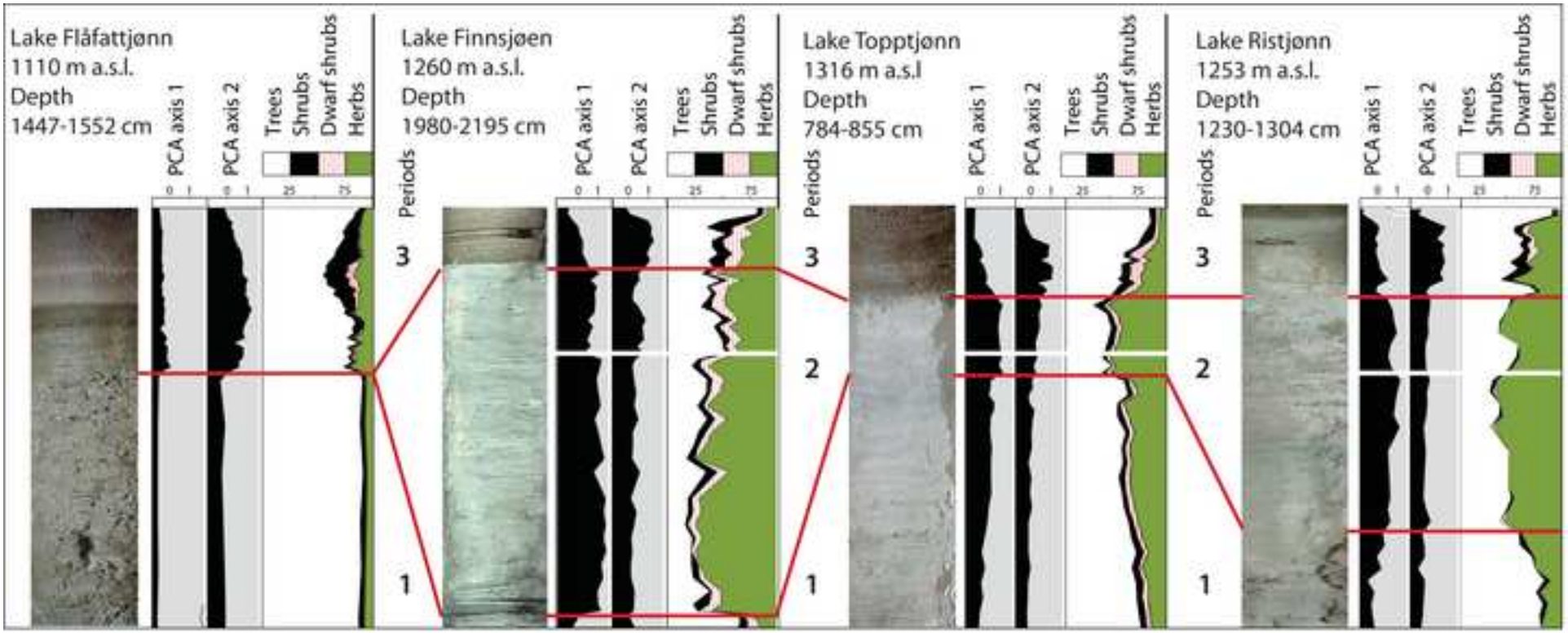

Figure 9. BW

Click here to download high resolution image

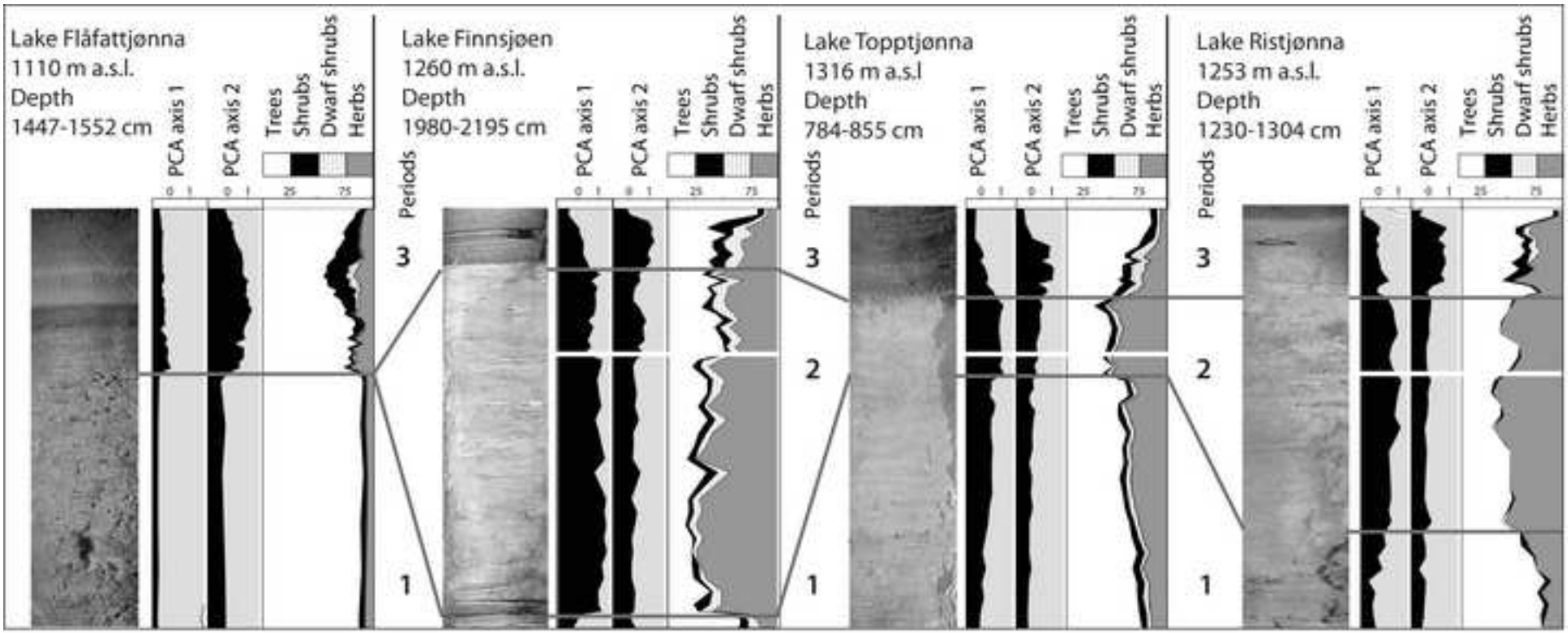

Figure 10

Click here to download high resolution image

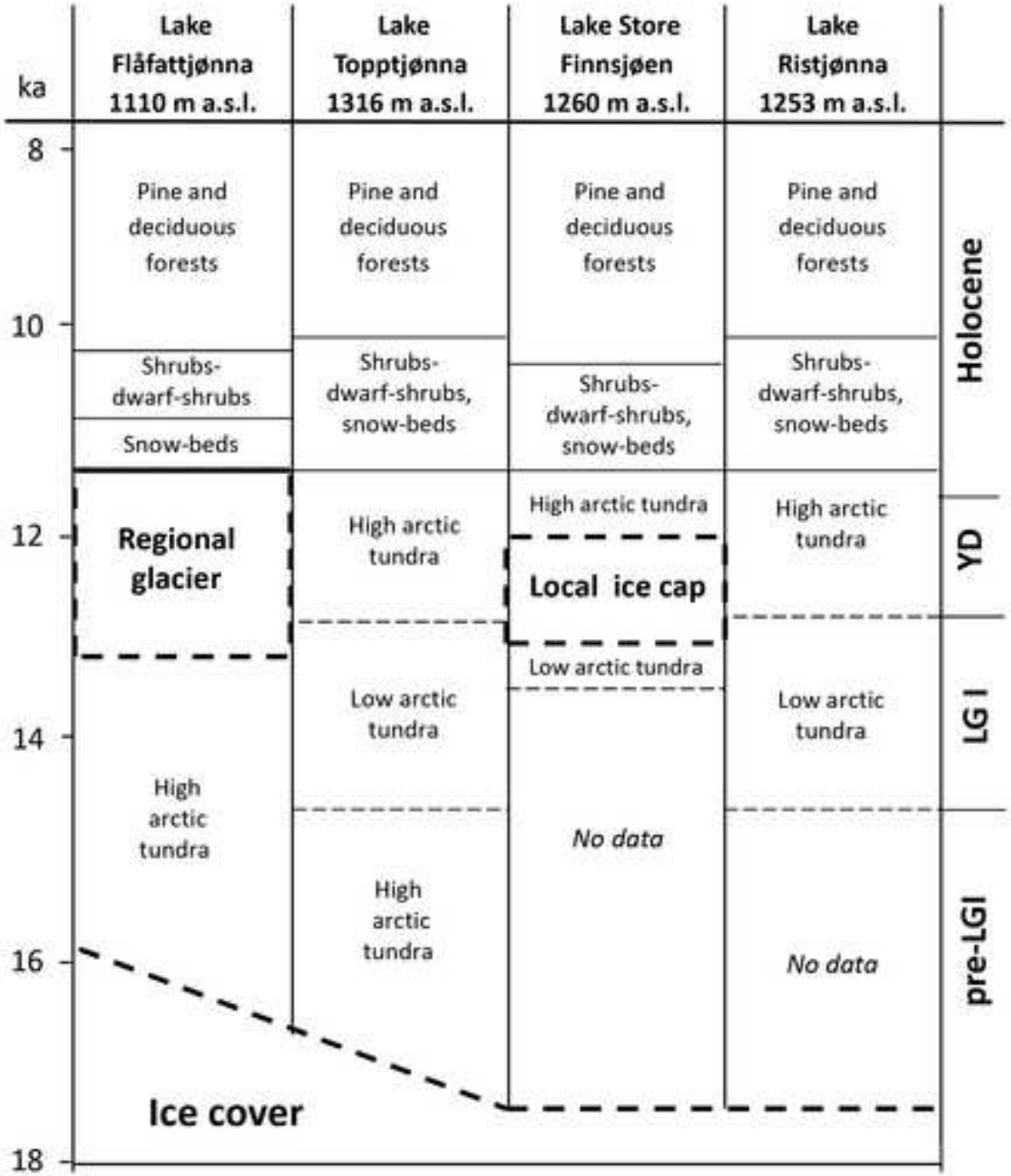

Appendix A

Click here to download Supplementary Data: AppendixA.doc

AppendixB.doc

Click here to download Supplementary Data: AppendixB.doc

AppendixC.doc

Click here to download Supplementary Data: AppendixC.doc